Title

Gain-of-Function RHOA Mutations Promote Focal Adhesion Kinase Activation and Dependency in Diffuse Gastric Cancer

Journal

Cancer Discovery, 10(2)

ISSN

2159-8274

Authors

Zhang, Haisheng
Schaefer, Antje
Wang, Yichen
et al.

Publication Date

2020-02-01

DOI

10.1158/2159-8290.cd-19-0811

Peer reviewed

Published in final edited form as:

Cancer Discov. 2020 February ; 10(2): 288–305. doi:10.1158/2159-8290.CD-19-0811.

Gain-of-Function RHOA Mutations Promote Focal Adhesion Kinase Activation and Dependency in Diffuse Gastric Cancer

Haisheng Zhang[1,2,*], **Antje Schaefer**[3,4,*], **Yichen Wang**[2], **Richard G. Hodge**[3], **Devon R. Blake**[4], **J. Nathaniel Diehl**[5], **Alex G. Papageorge**[8], **Matthew Stachler**[2], **Jennifer Liao**[2], **Jin Zhou**[2], **Zhong Wu**[2], **Fahire Akarca**[2], **Leonie K. de Klerk**[2], **Sarah Derks**[2], **Mariaelena Pierobon**[11], **Katherine A. Hoadley**[3,5,6], **Timothy C. Wang**[9], **George Church**[12], **Kwok-Kin Wong**[10], **Emanuel F. Petricoin**[11], **Adrienne D. Cox**[3,4,7], **Douglas R. Lowy**[8], **Channing J. Der**[3,4,5,#], **Adam J. Bass**[2,13,#]

[1]Department of General Surgery, Nanfang Hospital, Southern Medical University, Guangzhou, China

[2]Division of Molecular and Cellular Oncology, Dana-Farber Cancer Institute, Harvard Medical School, Boston, MA, USA

[3]Lineberger Comprehensive Cancer Center, University of North Carolina at Chapel Hill, Chapel Hill, NC, USA

[4]Department of Pharmacology, University of North Carolina at Chapel Hill, Chapel Hill, NC, USA

[5]Curriculum in Genetics and Molecular Biology, University of North Carolina at Chapel Hill, Chapel Hill, NC, USA

[6]Department of Genetics, University of North Carolina at Chapel Hill, Chapel Hill, NC, USA

[7]Department of Radiation Oncology, University of North Carolina at Chapel Hill, Chapel Hill, NC, USA

[8]Laboratory of Cellular Oncology, National Cancer Institute, National Institutes of Health, Bethesda, MD, USA

[9]Division of Gastroenterology, Columbia University Medical Center, New York, NY, USA

[10]Division of Hematology and Oncology, New York University, New York, NY, USA

[11]Center for Applied Proteomics and Molecular Medicine, School of Systems Biology, George Mason University, Manassas, VA, USA

Correspondence to Adam J. Bass, M.D., Dana-Farber Cancer Institute, 450 Brookline Ave; Dana 810B, Boston, MA 02215, 617-632-2477, (adam_bass@dfci.harvard.edu), Or Channing J. Der, Ph.D., Lineberger Comprehensive Cancer Center, University of North Carolina at Chapel Hill, Chapel Hill, NC 27514, 919-966-5634 (channing_der@med.unc.edu).

*These authors contributed equally

#These authors contributed equally

Authors' Contributions

A.J.B., H.Z., C.J.D., A.S. and D.R.L. designed the study and experiments. A.J.B., C.J.D., E.F.P., T.C.W., and D.R.L. provided resources and critical input. K.K.W oversaw generation of the novel murine allele. Methodology: A.S., R.G.H., D.R.B. and J.N.D. conducted the biochemical and cell culture experiments, A.G.P. performed metabolic labeling, H.Z. and Y.W. performed the organoid experiments, M.P. performed the RPPA studies and H.Z.,Y.W., J.L. and J.Z. conducted the *in vivo* experiments. Formal Analyses: A.S., R.G.H. and D.R.B. conducted the biochemical analyses, J.N.D. analyzed the RPPA results. M.S. and A.F. provided pathology expertise. L.K. and S.D. provided human DGC samples for the IHC staining. Writing – Original Draft, A.J.B., H.Z., A.S., R.G.H., K.A.H., J.N.D., A.D.C. and C.J.D.; Writing – Review & Editing, A.J.B., H.Z., A.S., R.G.H., D.R.B., A.D.C., D.R.L.,G.C. and C.J.D.

[12]Harvard, MIT, Blavatnik Inst., Wyss Inst., Boston, MA, USA

[13]Broad Institute of MIT and Harvard, Cambridge, MA, USA

Abstract

Diffuse gastric cancer (DGC) is a lethal malignancy lacking effective systemic therapy. Among the most provocative recent results in DGC has been that of highly recurrent missense mutations in the GTPase RHOA. The function of these mutations has remained unresolved. We demonstrate that $RHOA^{Y42C}$, the most common RHOA mutation in DGC, is a gain-of-function oncogenic mutant and that expression of $RHOA^{Y42C}$ with inactivation of canonical tumor suppressor *Cdh1* induces metastatic DGC in a mouse model. Biochemically, $RHOA^{Y42C}$ exhibits impaired GTP hydrolysis and enhances interaction with its effector ROCK. *RHOA*^{Y42C} mutation and *Cdh1* loss induce actin/cytoskeletal rearrangements and activity of focal adhesion kinase (FAK), which activates YAP/TAZ, phosphoinositide 3-kinase (PI3K)/AKT and β-catenin. $RHOA^{Y42C}$ murine models were sensitive to FAK inhibition and to combined YAP and PI3K pathway blockade. These results, coupled to sensitivity to FAK inhibition in patient-derived DGC cell lines, nominate FAK as a novel target for these cancers.

Keywords

RHOA mutation; Focal Adhesion Kinase; YAP/TAZ; β-catenin; Diffuse Gastric Cancer

INTRODUCTION

Gastric cancer (GC), the third leading cause of cancer death world-wide (1), is classically divided into two histologic types, intestinal and diffuse (2). Histologically, diffuse GC (DGC) is notable for the frequent appearance of mucin-filled ‘signet-ring’ cells, highly invasive and poorly differentiated cancer cells, lack of cellular cohesion (3), and an invasive growth pattern that contributes to rapid invasion and peritoneal metastases. Molecularly, DGCs largely fall into Genomically Stable molecular group, tumors typically lacking hypermutation and chromosomal instability (4). The absence of mutations in conventional oncoproteins and uncertainty over mechanisms of transformation in DGC have hindered therapeutic development. The most specific genomic aberration in sporadic DGC, whether through mutation (5) or methylation (6,7), is somatic inactivation of the tumor suppressor gene *CDH1*, which encodes the adhesion protein E-cadherin. In hereditary DGC, *CDH1* is inactivated in the germline (8,9). More recently, genomic characterization by our group and others (3,4,10–12) identified missense mutations of RAS homologous (RHOA) small GTPase in 15–26% of DGC.

Like RAS, RHOA cycles between inactive, GDP-bound and active GTP-bound conformations, the latter of which interacts with downstream effectors to regulate the actin cytoskeleton, cell migration, cytokinesis and the cell cycle (13). Yet, RHOA missense mutations in DGC occur at residues distinct from conventional activating mutations found in RAS (Supplementary Fig. S1A). Neither the consequences of these mutations for RHOA activity nor their impacts on disease pathogenesis have been clearly established. Studies of

RHOA mutations in DGC have reached conflicting conclusions. Kakiuchi *et al.* described recurrent *RHOA* mutations as gain-of-function; siRNA-mediated silencing of *RHOA* reduced proliferation in non-DGC cancer cells harboring *RHOA* mutations (3). In contrast, Wang *et al.* suggested that $RHOA^{Y42C}$ is a loss-of-function mutant, as ectopic $RHOA^{Y42C}$ attenuated GTP-levels, inferred from cell-based pulldown analyses using the RHOA-GTP binding domain (RBD) of Rhotekin (10).

In this study, we characterized the $RHOA^{Y42C}$ mutation via extensive biochemical analyses and detailed investigation of its activity in gastric epithelium using a genetically-engineered mouse model (GEMM). We demonstrate that recurrent genomic alterations found in DGC, *CDH1* loss coupled with $RHOA^{Y42C}$, induces metastatic DGC in mice resembling the human disease. Using detailed biochemistry, we established that the Y42C mutation activates RHOA, impairing GTP hydrolysis and promoting RHOA interaction with ROCK, and enhancing actin rearrangements and focal adhesion formation. Furthermore, we demonstrate that *Cdh1* loss and $RHOA^{Y42C}$ induce DGC via activation of focal adhesion kinase (FAK), promoting activation of YAP/TAZ, PI3K/AKT and β-catenin, thereby identifying therapeutic approaches for DGC. FAK inhibition abrogates tumor growth in our novel model and shows efficacy across a broader panel of patient-derived DGC cell lines, suggesting that FAK may serve as a potent therapeutic target for these cancers.

RESULTS

Cdh1 Loss with RHOA-Y42C Induces Diffuse Gastric Cancer *In Vivo*

Given the lack of DGC cell lines harboring *RHOA* mutations, we chose to study RHOA mutation in the gastric lineage by establishing a murine model, *LSL-*$RHOA^{Y42C}$ (using Y42C, the most recurrent RHOA mutation in DGC, Supplementary Fig. S1A), with *RHOA* ^{Y42C} engineered into the *Col1A1* locus where its expression is activated by Cre recombinase (Fig. 1A). We introduced the *Mist1*-CreERT2 allele to express tamoxifen-activated Cre in the *Mist1* locus, a marker of gastric chief cells suggested to be expressed in isthmus stem cells (14–16). To represent the most common genomic aberration in DGC, loss of *CDH1*, we used a conditional *Cdh1* allele, $Cdh1^{Flox/Flox}$. Finally, the *R26*-mTmG 'Tomato-GFP' allele was introduced to mark Cre-recombined cells by conversion from Tomato (red) to GFP (green). We bred cohorts of mice where we could inducibly express $RHOA^{Y42C}$ in gastric epithelium and inducibly inactivate *Cdh1,* either alone or in combination.

While we aged mice following *in vivo* induction of Cre activity, we developed murine gastric organoids to evaluate $RHOA^{Y42C}$ activity. Recombination was induced in the organoids *in vitro* via tamoxifen or adenoviral Cre-recombinase, and validated by conversion of Tomato to GFP expression (Fig. 1A), immunoblotting and immunofluorescence (Supplementary Fig. S1B–S1E). Following induction, we observed dramatic morphologic changes and induction of mesenchymal markers (Fig. 1B and C; Supplementary Fig. S1D–S1F and Supplementary Video S1) in organoids expressing $RHOA^{Y42C}$ in the absence of *Cdh1* ($Cdh1^{-/-}RHOA^{Y42C/+}$: *Mist1*-CreERT2, $Cdh1^{Flox/Flox}$, *LSL-*$RHOA^{Y42C/+}$), but not with $RHOA^{Y42C/+}$ alone ($RHOA^{Y42C/+}$: *Mist1*-CreERT2, *LSL-*$RHOA^{Y42C/+}$) or *Cdh1* loss alone ($Cdh1^{-/-}$: *Mist1*-CreERT2, $Cdh1^{Flox/Flox}$). Whereas $Cdh1^{-/-}$ or $RHOA^{Y42C/+}$ organoids retained spherical forms with hollow interiors, $Cdh1^{-/-}RHOA^{Y42C/+}$ organoids

exhibited abnormal morphology and central filling (Fig. 1B and C), a phenotype associated with transformation and consistent with morphologies of patient-derived DGC organoids (12,17). Histologic review identified signet-ring cells, a characteristic feature of DGC, in *Cdh1*$^{-/-}$*RHOA*$^{Y42C/+}$ organoids (Fig. 1D; Supplementary Fig. S1G).

To determine if these organoids were transformed, we transplanted them (5×10^5 cells) via surgical injection into gastric walls of *NOD.Cg-Prkdc*^{scid} *Il2rg*^{tm1Wjl}*/SzJ* (NSG) mice (Fig. 1E). Mice implanted with *Cdh1*$^{-/-}$*RHOA*$^{Y42C/+}$ organoids formed tumors and exhibited peritoneal spread, ascites and metastases to lung and liver (Fig. 1F and G). By contrast, no tumors formed with *Cdh1*$^{-/-}$ or *RHOA*$^{Y42C/+}$ or *Mist1*Cre control organoids. Accordingly, survival analysis showed that mice implanted with *Cdh1*$^{-/-}$*RHOA*$^{Y42C/+}$ organoids succumbed rapidly whereas survival was not decreased in other groups (Fig. 1H). We obtained analogous results following subcutaneous flank injections (Supplementary Fig. S1H and S1I).

We then evaluated autochthonous expression of *RHOA*^{Y42C} in mice aged for 14 months after *in vivo* tamoxifen induction. Tumors were identified in the stomachs only of *Cdh1*$^{-/-}$*RHOA*$^{Y42C/+}$ mice (5/8 mice, 62.5%; Supplementary Fig. S1J). These results recapitulate those showing that *Mist1*-CreERT2, *Cdh1*$^{Flox/Flox}$ mice do not develop tumors unless infected with *Helicobacter felis* (16). Histologic analysis confirmed that *Cdh1*$^{-/-}$*RHOA*$^{Y42C/+}$ tumors were poorly differentiated with cells resembling signet-ring cells (Supplementary Fig. S1K). These results establish *RHOA*^{Y42C} as an oncogene that, with *Cdh1* loss, induces tumors resembling human DGC.

RHOA^{Y42C} Exhibits A Gain-of-Function Phenotype *In Vitro*

We next characterized consequences of the Y42C mutation for RHOA function by assessing its effect on RHOA-regulated cellular activities. Seminal studies establishing involvement of RHOA in regulating actin cytoskeletal organization, cell adhesion and migration utilized lab-generated, constitutively-activated RHOA mutants (G14V, Q63L; analogous to RAS residues G12 and Q61) expressed in NIH/3T3 mouse fibroblasts and related 3T3 cell lines (18,19). To evaluate the activity of RHOA^{Y42C} relative to extensive literature evaluating RHOA variants in NIH/3T3 cells we established NIH/3T3 cells stably expressing exogenous RHOA^{Y42C} protein at levels comparable to exogenous RHOA^{WT} or RHOA^{Q63L} (Supplementary Fig. S2A and S2B). NIH/3T3 fibroblasts are mesenchymal cells lacking expression of the epithelial cell-restricted CDH1 gene.

RHOA promotes actin stress fibers, which are important for cell morphology and adhesion. As we described previously (20), RHOA^{Q63L} enhanced stress fiber formation compared with RHOA^{WT} (Fig. 2A and B). RHOA^{Y42C} also enhanced stress fiber formation, at a level intermediate between Q63L and WT, indicating that Y42C causes a gain-of-function phenotype with respect to this canonical RHOA function.

RHOA also stimulates focal adhesions (FA) assembly, protein complexes that connect the actin cytoskeleton with the extracellular matrix (21,22) We investigated the ability of RHOA^{Y42C} to regulate FA assembly in NIH/3T3 cells, utilizing the Focal Adhesion Analysis Server. Both RHOA^{Q63L} and RHOA^{Y42C} but not RHOA^{WT} increased FA size

(area, Fig. 2C). Conversely, $RHOA^{WT}$ reduced the numbers of FA per cell, whereas $RHOA^{Y42C}$ did not (Fig. 2D). $RHOA^{Q63L}$ but not $RHOA^{WT}$ enhanced FA eccentricity (deviation from a circular shape, Fig. 2E). Although the increase did not reach statistical significance, $RHOA^{Y42C}$ also enhanced FA eccentricity (Fig. 2E). We conclude that like $RHOA^{Q63L}$, $RHOA^{Y42C}$ exhibits a gain-of-function phenotype with respect to FA assembly.

We next evaluated the ability of $RHOA^{Y42C}$ to regulate cell-matrix adhesion. As previously reported, $RHOA^{Q63L}$ impaired adhesion to fibronectin (Fig. 2F). Surprisingly, $RHOA^{WT}$ also impaired adhesion, whereas $RHOA^{Y42C}$ did not. Thus, the effect of $RHOA^{Y42C}$ on adhesion differs from both WT and Q63L. Actin stress fiber and FA organization regulate cell migration (22). As shown previously (23,24), $RHOA^{Q63L}$ impaired the velocity (Fig. 2G) and directionality of migration (Supplementary Fig. S2C). In contrast, $RHOA^{Y42C}$-expressing cells showed similar migration velocity and directionality as WT.

We then evaluated these findings in our murine gastric organoids, in which we could induce *Cdh1* loss and/or $RHOA^{Y42C}$ expression (overview of models used in this study in Supplementary Table S1). Immunofluorescence microscopy studies revealed increased F-actin levels in $RHOA^{Y42C/+}$ organoids (especially in $Cdh1^{-/-}RHOA^{Y42C/+}$ organoids) compared to *Mist1*Cre or $Cdh1^{-/-}$ organoids (Fig. 2H), consistent with our NIH/3T3 results (Fig. 2A and B).

Overall, our studies of actin- and FA-mediated cell adhesion and migration show that $RHOA^{Y42C}$ causes a gain-of-function phenotype that does not simply phenocopy lab-generated constitutively-activated mutant $RHOA^{Q63L}$. It has been a puzzle as to why RHOA mutations analogous to RAS are not found in cancer. Our results suggest a possible clue: the lab-generated $RHOA^{Q63L}$ mutant may reduce actin dynamics by overly increasing stress fiber formation thus decreasing rather than increasing motility. In contrast, $RHOA^{Y42C}$ may optimally increase both stress fiber formation and motility to more effectively engage the actin cytoskeleton in a pro-transformation manner.

$RHOA^{Y42C}$ Exhibits Impaired GTP Hydrolysis and Altered Effector Binding

We next determined the mechanistic basis for the gain-of-function biochemical Y42C phenotype. We initially hypothesized that, like the cancer-associated RAC1b splice variant that is impaired in RhoGDI1 interaction (25), the Y42C mutation impairs RHOA interaction with RhoGDI1, a regulator of membrane association and subcellular localization (13). We ectopically co-overexpressed HA-epitope-tagged RHOA and GFP-tagged RhoGDI1 in COS-7 cells, immunoprecipitated HA-RHOA, and immunoblotted for GFP. In agreement with previous studies (26,27), we found that $RHOA^{WT}$ but not active $RHOA^{Q63L}$ or the $RHOA^{T19N}$ dominant-negative mutant associated with RhoGDI1 (Supplementary Fig. S2D and S2E). However, $RHOA^{Y42C}$ binding to RhoGDI1 was similar to that of $RHOA^{WT}$. Consistent with this, $RHOA^{Y42C}$ and $RHOA^{WT}$ displayed similar subcellular localization in NIH/3T3 cells (Supplementary Fig. S2F). We conclude that Y42C does not alter RHOA interaction with RhoGDI1.

We next hypothesized that Y42C imparts a fast-cycling phenotype, like the gain-of-function, cancer-associated P29S mutation in the small GTPase RAC1 (28). We purified *E. coli*-

expressed recombinant RHOA proteins and measured intrinsic nucleotide exchange using a fluorescence-labelled-nucleotide assay. However, activities of RHOA WT and Y42C were not significantly different (Fig. 3A). Thus, Y42C does not alter GDP-GTP cycling.

To evaluate Y42C interaction with GEFs, we evaluated TCGA data for expression of RHO family GEFs and GAPs in gastric cancer (Supplementary Fig. S3A). The RHOA-selective GEF *ECT2* is preferentially upregulated in GC compared to adjacent normal tissue (Supplementary Fig. S3B). ECT2 overexpression is associated with GC progression and poor prognosis (29). Therefore, we tested the ability of recombinant ECT2 C-terminal DH-PH domain (catalytic GEF fragment) to stimulate nucleotide exchange on WT and mutant RHOA. ECT2-catalyzed nucleotide exchange activities on $RHOA^{WT}$ and $RHOA^{Y42C}$ were similar to each other (kcat = 23.3×10^{-4} s^{-1} and 21.1×10^{-4} s^{-1}, respectively, Fig. 3B; Supplementary Fig. S3C), and to activities described for other RhoGEFs (30), indicating that Y42C does not alter GEF sensitivity.

Activating RAS mutations (e.g., Q61L) impair intrinsic and GAP-stimulated GTP hydrolysis, thereby favoring the active, GTP-bound form. We directly measured GTP bound to recombinant RHOA proteins in HPLC assays. The intrinsic GTP hydrolysis rate, which was completely abolished by the Q63L mutation (Fig. 3C and D), was reduced 440-fold in $RHOA^{Y42C}$ relative to $RHOA^{WT}$ (0.05×10^{-5} s^{-1} and 22.1×10^{-5} s^{-1}, respectively). To verify this striking GTPase deficiency, we also applied a fluorescence-based hydrolysis assay using a phosphate-binding-protein sensor, which confirmed that intrinsic GTP hydrolysis is greatly impaired in $RHOA^{Y42C}$ (Fig. 3E and F). Finally, since Y42C is located in the switch I region of RHOA, which is also involved in GAP binding, we performed precise biochemical assays to determine whether Y42C alters GAP activation. Using recombinant protein (catalytic domain only) of the RHOA-specific GAP p190RhoGAP/ARHGAP35, expressed at high levels in GC (Supplementary Fig. S3A), we found that GAP-stimulated catalytic activity of $RHOA^{Y42C}$ was reduced 4-fold relative to $RHOA^{WT}$ (kcat = 2.6×10^{-2} s^{-1} and 10.4×10^{-2} s^{-1}, respectively; Fig. 3G; Supplementary Fig. S3D). These results indicate that reductions in both intrinsic and GAP-stimulated GTP hydrolysis favor increased levels of $RHOA^{Y42C}$-GTP.

To directly measure the guanine nucleotide bound to $RHOA^{Y42C}$ in living cells, we adapted the classic method of ^{32}P-orthophosphate metabolic labeling developed originally for RAS. Unlike the standard pulldown assay that detects only relative levels of RHOA-GTP (21), the ^{32}P radiolabeling assay enables precise quantitation of the percentage of RHOA bound to GTP or GDP. As expected, RHOA WT was predominantly GDP-bound (only 1.8% GTP-bound; Fig. 3H; Supplementary Fig. S3E), whereas $RHOA^{Q63L}$ was predominantly (78%) GTP-bound. Surprisingly, despite its impaired GTP hydrolysis, Y42C showed a reproducible but not statistically significant increase in GTP binding (3.2%) compared to $RHOA^{WT}$. This result suggests that additional alterations other than those tilting the balance of GTP to GDP contribute to the ability of $RHOA^{Y42C}$ to stimulate canonical RHOA functions such as actin stress fiber and FA formation.

Y42 lies in RHOA's effector domain. Studies performed prior to discovery of *RHOA* mutations in DGC showed that a Y42C substitution generated in *cis* with RAS-like

activating RHOA mutations (G14V or Q63L) altered RHOA effector interactions (31,32). However, how Y42C alone impacts effector interactions has not been determined. ROCK and mDia are RHOA effector proteins regulating F-actin dynamics (33), and Rhotekin-RBD is the standard pulldown reagent used to determine RHOA-GTP levels in cells (21). Utilizing a well-established fluorescence-based effector interaction assay, we found that the binding affinities between recombinant $RHOA^{WT}$ and the isolated RBDs of Rhotekin (500 ± 40 nM), ROCK (380 ± 30 nM) and mDia (460 ± 60 nM) were similar to each other (Supplementary Fig. S3F) and comparable to previous studies (34,35). In contrast, whereas $RHOA^{Y42C}$ binding to mDia-RBD was comparable to that of $RHOA^{WT}$, its binding to ROCK-RBD was increased 12-fold (Fig. 3I; Supplementary Fig. S3F). Unexpectedly, $RHOA^{Y42C}$ did not bind to Rhotekin-RBD, indicating that the standard Rhotekin-RBD pulldown assay does not accurately measure GTP levels of Y42C. Mechanistically, since ROCK promotes actin stress fiber formation, whereas Rhotekin has been reported to antagonize it (36), the enhanced ROCK binding of $RHOA^{Y42C}$ together with loss of Rhotekin binding provides further basis for its gain-of-function phenotype observed in stress fiber formation assays (Fig. 2A and B). Additionally, since ROCK enhances FA formation (37), increased ROCK binding may contribute to the gain-of-function phenotype of $RHOA^{Y42C}$ in our FA studies. Taken together with its impaired intrinsic and GAP-stimulated GTP hydrolysis, we demonstrated that $RHOA^{Y42C}$ is a gain-of-function mutant due to alterations in both GDP-GTP regulation and effector interactions (see model, Fig. 3J). These results suggest a biochemical basis for $RHOA^{Y42C}$ serving as a driver of DGC in our mouse model.

RHOAY42C Promotes Activation of PI3K/AKT, β-catenin and YAP/TAZ

Having established that $RHOA^{Y42C}$ is an oncogene, we next evaluated the signaling and cellular effects of $RHOA^{Y42C}$ expression in the gastric lineage. We established a isogenic organoids from the gastric epithelia of $Cdh1^{Flox/Flox}$ mice (Supplementary Fig. S4A and S4B). We introduced ectopic EGFP-$RHOA^{Y42C}$, EGFP-$RHOA^{Q63L}$, EGFP-$RHOA^{WT}$ or EGFP control via lentiviral transduction and created either *Cdh1*-null or WT models by using adenoviral Cre recombinase. These organoids were then evaluated by Reverse Phase Protein Array (RPPA) analyses to evaluate the consequences of genetic alterations on global signaling. Analyses revealed increased phosphorylation of diverse signaling proteins in *Cdh1*-null organoids expressing $RHOA^{Y42C}$ compared to $RHOA^{WT}$ (Supplementary Fig. S4C and Supplementary Table S2). These differences were markedly increased in *Cdh1*-null compared to isogenic *Cdh1* WT organoids. Consistent with our biochemical and cellular analyses, RPPA identified ROCK activation in *Cdh1*-null organoids expressing $RHOA^{Y42C}$ compared to $RHOA^{WT}$ (Fig. 4A; Supplementary Fig. S4D). Increased activation of PI3k-AKT-mTORC1 signaling in *Cdh1*-null $RHOA^{Y42C}$ expressing organoids was also observed (Fig. 4A; Supplementary Fig. S4E). AKT phosphorylation at S473 and T308 were two of the most significantly upregulated phosphorylation sites in *Cdh1*-null organoid with exogenous $RHOA^{Y42C}$ versus $RHOA^{WT}$ (Fig. 4B). Many significant changes found in *Cdh1*-null organoids were not observed with *Cdh1* WT organoids (Fig. 4C), suggesting that signaling required to induce tumor formation is dependent on both *Cdh1* loss and $RHOA^{Y42C}$ expression (Fig. 1).

Interestingly, the EGFP-RHOA^{Q63L} vector could not be expressed in *Cdh1* intact organoids. Although *Cdh1*-null organoids expressing RHOA^{Q63L} showed the same increased AKT phosphorylation at S473 as with RHOA^{Y42C}, the overall signaling profile was distinct (Supplementary Fig. S4F and S4G). These findings together with our biochemical and cellular studies may provide evidence for why RHOA^{Q63L} is not found in cancer.

Because of the RPPA results, we focused on further evaluation of AKT signaling. Immunoblotting confirmed that AKT was not activated in *Cdh1*-null organoids unless RHOA^{Y42C} was also expressed (Fig. 4D). Under those conditions, we also observed elevated phosphorylation of AKT target Gsk3β at S9 (Fig. 4D), which downregulates destruction of β-catenin by the Gsk3β/Axin/APC complex (38–40). Immunoblotting also demonstrated that β-catenin abundance was markedly attenuated in *Cdh1*$^{-/-}$ compared to *Cdh1*$^{+/+}$ organoids and was not altered upon expression of RHOA^{WT} (Fig. 4D). In contrast, RHOA^{Y42C} increased β-catenin expression in *Cdh1*-null organoids. E-cadherin tethers β-catenin to the cell membrane. Thus, we hypothesized that the combination of GSK3β repression and loss of *Cdh1*/E-cadherin enables nuclear translocation β-catenin in *Cdh1*$^{-/-}$*RHOA*$^{Y42C/+}$ organoids. Indeed, these organoids displayed elevated nuclear β-catenin *in vitro* and following orthotopic implantation (Fig. 4E; Supplementary Fig. S4H–S4J). We further validated that downstream targets of β-catenin, c-Myc and Cyclin D1 were upregulated by RHOA^{Y42C} expression (Supplementary Fig. S4K). To investigate the relationship of AKT activation and β-catenin induction, we ectopically expressed the constitutively-activated mutant PI3Kα^{H1074R} (PIK3CA^{H1074R}) in *Cdh1*-null organoids and observed increased levels of pAKT and active β-catenin (Supplementary Fig. S4L). Conversely, pharmacologic blockade of PI3K (with pictilisib) or AKT (with MK-2206) suppressed the TOP/FOP Wnt/β-catenin reporter in *Cdh1*$^{-/-}$*RHOA*$^{Y42C/+}$ organoids (Supplementary Fig. S4M). These data demonstrate that, in the setting of *Cdh1* loss, RHOA-mediated PI3K activation promotes β-catenin activation.

We next sought additional mediators of RHOA's oncogenic activity. RHOA mediates activation of YAP/TAZ (41,42), which interacts with β-catenin (43). We found expressing RHOA^{Y42C} in *Cdh1*-null organoids increased YAP and TAZ expression (Fig. 4F) and active, non-phosphorylated form YAP (Fig. 4G), suggesting that YAP/TAZ signaling is activated in *Cdh1*$^{-/-}$*RHOA*$^{Y42C/+}$ organoids. As RHOA^{Y42C} activates both β-catenin and YAP/TAZ signaling, we evaluated whether activation of these pathways replaces RHOA^{Y42C} in mediating transformation of *Cdh1*-null gastric organoids. Although expression of either active YAP(S127A) (Supplementary Fig. S4N) or β-catenin(S33Y) alone failed to induce tumor growth, combination of both YAP(S127A) and β-catenin(S33Y) induced robust tumor formation (Fig. 4H) with cells resembling signet ring cells both in vitro and following xenograft growth (Supplementary Fig. S4O and S4P).

YAP/TAZ and β-catenin Pathways Are both Required for *Cdh1*$^{-/-}$*RHOA*$^{Y42C/+}$-Induced Transformation

We next investigated whether the YAP/TAZ and β-catenin pathways are necessary for RHOA^{Y42C} oncogenicity. We first targeted these pathways with genetic tools in *Cdh1*$^{-/-}$*RHOA*$^{Y42C/+}$ organoids, using the YAP dominant negative mutant S94A (YAP-DN,

Supplementary Fig. S5A) and a dominant negative mutant of β-catenin cofactor TCF4 (TCF4-DN, aa 1–31 del; Supplementary Fig. S5B). Although only YAP-DN inhibited organoid growth *in vitro*, both attenuated the aberrant organoid morphology (Supplementary Fig. S5C and S5D). Importantly, either YAP-DN or TCF4-DN dramatically inhibited tumor growth *in vivo* (Fig. 5A–B; Supplementary Fig. S5E). Histological analyses showed that small tumors formed following expression of YAP-DN or TCF4-DN displayed less resemblance to DGC and instead displayed greater gland formation and differentiation (Fig. 5C). To determine if YAP-DN or TCF4-DN also inhibit organoid-derived gastric cancer models that were not driven by *Cdh1* loss and $RHOA^{Y42C}$, we utilized a model generated from $Trp53^{-/-}Kras^{G12D/+}$ mice (44). We found only modest effects on tumor growth and *in vitro* proliferation of $Trp53^{-/-}Kras^{G12D/+}$ organoids similarly engineered to express YAP-DN and/or TCF4-DN (Fig. 5D; Supplementary Fig. S5F), demonstrating that targeting these pathways did not induce nonspecific toxicity. Overall, these data suggest that the YAP/TAZ and β-catenin/TCF4 pathways are necessary and sufficient to drive tumor formation in the $Cdh1^{-/-}RHOA^{Y42C/+}$ gastric model.

We next explored the therapeutic potential of pharmacologically targeting these pathways in $Cdh1^{-/-}RHOA^{Y42C/+}$ organoids. We targeted the AKT/β-catenin axis with ICG-001, an antagonist of β-catenin cofactor TCF4, or with AKT inhibitor MK-2206, both of which attenuated aberrant organoid morphology and had modest but significant effects on viability (Supplementary Fig. S5G–S5I). Similarly, YAP pathway inhibitor verteporfin had modest effects on organoid proliferation (Supplementary Fig. S5I). Further testing suggested that pharmacological inhibition of single pathways led to adaptive changes in other pathways, which may mitigate responses to single drug treatment (Supplementary Fig. S5J). Specifically, YAP/TAZ inhibition induced pAKT; conversely, AKT inhibition enhanced TAZ expression. Accordingly, the combination of verteporfin with either ICG-001 or MK-2206 markedly inhibited proliferation and induced apoptosis in the $Cdh1^{-/-}RHOA^{Y42C/+}$ model (Fig. 5E and F; Supplementary Fig. S5G), whereas the same treatments had only modest effects on organoids from $Trp53^{-/-}Kras^{G12D/+}$ mice (Fig. 5E and F; Supplementary Fig. S5I and S6A). We also tested these combinations in normal and $Cdh1^{-/-}$ organoids, finding only a modest effect relative to their effects in the $Cdh1^{-/-}RHOA^{Y42C/+}$ model (Supplementary Fig. S5K and S5L).We next tested these combinations *in vivo* in the transplanted $Cdh1^{-/-}RHOA^{Y42C/+}$ model. Instead of ICG-001, we inhibited the PI3K/AKT pathway, given the availability of drugs in advanced clinical development. Our *in vitro* studies showed that PI3K inhibitor pictilisib, which inhibits AKT, to be superior to MK-2206 (Supplementary Fig. S6B and S6C). We therefore selected pictilisib for *in vivo* combination with verteporfin. Both verteporfin and pictilisib individually inhibited tumor growth, and we saw greater effects with the combination (Fig. 5G; Supplementary Fig. S6D), suggesting clinical potential for combined PI3K/AKT- and YAP/TAZ-directed therapy in *RHOA*-mutant DGC.

$RHOA^{Y42C}$-mediated FAK activation induces PI3K/AKT and YAP/TAZ

We next investigated the more proximal means by which $RHOA^{Y42C}$ activates pathways including PI3K/AKT and YAP/TAZ. We hypothesized that Focal Adhesion Kinase (FAK) could mediate these activities because $RHOA^{Y42C}$ induces FA assembly and actin rearrangements, and activates PI3K/AKT signaling. FAK signaling has been described to

regulate FA dynamics, actin reorganization and PI3K/AKT signaling to drive invasion and metastasis and to contribute to RHOA activity in multiple cancers (45,46). Large-scale proteomic studies also implicated FAK-mediated pathways in human DGC (46,47). Our RPPA analyses revealed increased phosphorylation of FAK substrates (as pFAK was not in the RPPA panel) such as receptor tyrosine kinase Ret (48) in *Cdh1*-null organoids expressing $RHOA^{Y42C}$ (Fig. 4B).

By immunoblotting, we confirmed enhanced FAK activation upon $RHOA^{Y42C}$ expression in *Cdh1*-null organoids (Fig. 6A), and in $Cdh1^{-/-}RHOA^{Y42C/+}$ organoids (Fig. 6B; Supplementary Fig. S7A). Similarly, ectopic expression of WT *PTK2* (encoding FAK) in *Cdh1*-null organoids increased both pAKT and active YAP levels (Fig. 6C; Supplementary Fig. S7B). Furthermore, immunoprecipitation studies showed that FAK co-immunoprecipitated with PI3KCA in $Cdh1^{-/-}RHOA^{Y42C/+}$ organoids, indicating that FAK directly activates PI3K (Supplementary Fig. S7C). These results are consistent with studies on FAK-mediated PI3K/AKT activation controlling actin cytoskeletal remodeling and FA formation in multiple cancers (45,46). In addition, FAK also induced aberrant morphology in these organoids (Fig. 6D), recapitulating features seen with $RHOA^{Y42C}$, including mucin production which contributes to signet ring cell formation (Fig. 6E).

We then evaluated genetic and pharmacologic targeting of FAK in $Cdh1^{-/-}$ $RHOA^{Y42C/+}$ models. *sh*RNA-mediated silencing of *Ptk2* (FAK) reduced pAKT and active YAP (Fig. 6F; Supplementary Fig. S7D). Silencing of *Ptk2* (FAK) reverted the morphology of $Cdh1^{-/-}RHOA^{Y42C/+}$ organoids but had little effect on $Trp53^{-/-}Kras^{G12D/+}$ organoids (Supplementary Fig. S7E). We next evaluated pharmacologic FAK inhibition. PF-573228, a small molecule FAK inhibitor, attenuated activation of AKT, YAP and β-catenin (Fig. 6G; Supplementary Fig. S7F–S7H). PF-573228 treatment dramatically reversed the aberrant $Cdh1^{-/-}RHOA^{Y42C/+}$ morphology (Fig. 6H) in a dose-dependent manner (Supplementary Fig. S7I) and decreased staining with Ki67 (Supplementary Fig. S7J) and Alcian Blue, a marker of mucin formation (Fig. 6I). Live-cell confocal imaging demonstrated that PF-573228 normalized the morphology of $Cdh1^{-/-}RHOA^{Y42C/+}$ organoids over approximately 30 hours (Fig. 6J; Supplementary Video S2).

FAK Inhibition Abrogates both *In Vitro* Proliferation and *In Vivo* Tumor Growth

We next further explored FAK as a DGC therapeutic target. FAK inhibitor PF-573228 markedly decreased proliferation in $Cdh1^{-/-}RHOA^{Y42C/+}$ but not $Trp53^{-/-}Kras^{G12D/+}$ gastric organoids *in vitro* (Supplementary Fig. S7K and S7L), indicating FAK as specific target in our DGC model. We also found lack of efficacy in FAK inhibition in normal gastric organoids but greater effects of FAK inhibition in $Cdh1^{-/-}$ organoids, (Supplementary Fig. S7M–N) consistent with our finding of modestly enhanced pFAK following *Cdh1* loss (Supplementary Fig. S7O).Relatedly, PF-573228 abrogated tumor growth of $Cdh1^{-/-}RHOA^{Y42C/+}$ organoid xenografts (Fig. 6K). To validate our findings, we tested the clinical candidate FAK inhibitor, defactinib, and obtained similar results *in vitro* and *in vivo* (Fig. 6L; Supplementary Fig. S7P–S7R). To further characterize effects of FAK inhibition, we performed Ki67 and TUNEL staining of $Cdh1^{-/-}RHOA^{Y42C/+}$ organoid xenografts, finding evidence of both diminished proliferation and apoptosis induction (Fig. 6M–N).

Taken together, these results establish FAK as a mediator of $RHOA^{Y42C}$ function in DGC pathogenesis and establish this kinase as a promising candidate target (Fig. 6O).

FAK Is A Potent Therapeutic Target in Human DGC Cell Lines and Patients

We next evaluated FAK inhibition in human DGC cell line models. Although there are no DGC cell lines with endogenous RHOA mutation, RHOA activity has been demonstrated to be elevated in existing DGC cell lines relative to intestinal gastric cancer (IGC) models (49). Utilizing immunoblotting, we verified enhanced FAK activation in DGC lines compared to IGC lines (Fig. 7A and B). We checked E-cadherin in these DGC lines and found them either lacking E-cadherin expression (SNU668 and FU97) or possess CDH1 mutation (NUGC4 with CDH1, p.D257V) while IGC cell lines had markedly higher E-cadherin expression (Supplementary Fig. S8A). To further confirm our hypothesis that RHOA promotes FAK activation, we silenced RHOA using siRNA and observed attenuated pFAK levels (Supplementary Fig. S8B). We also found that FAK inhibitors PF-573228 and defactinib attenuated pFAK and pAKT levels in the DGC cell lines FU97 and SNU668, but not in IGC-line SNU719, which lacks evident pFAK (Fig. 7C). Furthermore, DGC lines were sensitive to PF-573228 treatment *in vitro* while IGC cells were insensitive (Fig. 7D and E). In DGC PF-573228 induced G2-M cell cycle arrest (Supplementary Fig. S8C) in dose-dependent manner (Supplementary Fig. S8D). We next compared *in vivo* growth of DGC SNU668 and IGC SNU719 cell lines. We found that DGC SNU668 tumor growth was inhibited by PF-573228 treatment, but had minimal response to 5-flourouracil (5-FU), a commonly used agent in DGC (Fig. 7F and G). In contrast, IGC line SNU719 showed markedly greater sensitivity *in vivo* to 5-FU compared to PF-5732228 (Fig. 7H; Supplementary Fig. S8E). PF-573228 treatment not only attenuated proliferation (Supplementary Fig. S8F), but also induced DNA damage and apoptosis of SNU668 in vivo (Supplementary Fig. S8G–S8H), consistent with data from organoids (Fig. 6M and 6N).

To further investigate FAK in DGC, we evaluated FAK activation in DGC surgical samples using immunohistochemistry, finding pFAK staining in 17 of 18 evaluated samples, with FAK staining in 70%−100% of tumor cells compared to negative staining in surface epithelial cells and minimal staining in normal glandular epithelial cells (Fig. 7I; Supplementary Fig. S8I). We also evaluated the level of pFAK in 8 non-DGC samples and observed positive staining in only one case (Supplementary Fig. S8J). These data provide support for the potential relevance of FAK in DGC beyond that observed in our engineered murine model.

DISCUSSION

Genomic studies of DGC have found that the two most characteristic classes of alterations affect cellular adhesion (e.g., *CDH1* and *CLND18*) and RHO signaling (e.g., *RHOA* and *ARHGAP26*) (4,12,50,51). However, these findings have yet to be translated to deeper functional understanding of disease pathogenesis or therapeutically. Whether *RHOA* mutations represent activating or inactivating alterations has remained uncertain. The specific residues recurrently mutated contributed to this uncertainty. $RHOA^{Y42C}$ is analogous to Y40C in RAS, an effector domain mutant impairing interaction of RAS^{G12V}

with RAF (52). Following these studies in RAS, RHOA Y42C had been studied in cis with activating RHOA mutations (G14V or Q63L) as an experimental strategy to attribute RHOA functions to specific RHOA effectors (31,32). Thus, when RHOA Y42C mutations were identified in DGC, it was unexpected that a putative loss-of-effector-function mutant could serve as an oncogene, fueling discussion whether RHOA serves as a tumor suppressor (3,10). Our analyses provide demonstrate $RHOA^{Y42C}$ to be an oncogene. Similar to $RHOA^{G14V/Q63L}$, $RHOA^{Y42C}$ exhibits an activated phenotype, stimulating actin stress fiber formation and FA assembly, albeit at a reduced potency. Interestingly, $RHOA^{Y42C}$ did not simply phenocopy $RHOA^{Q63L}$ but instead exhibited distinct activities in regulation of cell adhesion and migration, and signaling. That $RHOA^{Q63L}$ suppressed, whereas $RHOA^{Y42C}$ stimulated, migration is consistent with our finding that $RHOA^{Y42C}$ promotes DGC that is invasive and metastatic.

By studying $RHOA^{Y42C}$ without secondary mutations, we found impaired intrinsic and GAP-stimulated GTP hydrolysis activity, properties favoring formation of active GTP-bound RHOA. However, these biochemical defects did not drive significant steady-state accumulation of RHOA-GTP in cells. Our analyses of effector binding revealed additional alterations: increased affinity for ROCK, the key effector that drives RHOA stimulation of actin stress fibers and FA assembly, and loss of binding to Rhotekin, an effector that antagonizes actin stress fiber formation. Together, these altered effector interactions provide a mechanistic explanation for the $RHOA^{Y42C}$ gain-of-function phenotype, stimulating FA assembly and activation of FAK. Additionally, loss of Rhotekin binding explains why standard Rhotekin-RBD pulldown assays (21) would produce misleading results for $RHOA^{Y42C}$ activation.

Our murine gastric model provides further validation that $RHOA^{Y42C}$ is an oncogene. That oncogenic function was unmasked with loss of E-cadherin may explain why RHOA mutations are restricted to cancers arising from a very limited spectrum of tissue types. These results also suggest a functional interaction of RHOA and E-cadherin. Our data suggest gastric *CDH1* loss alone does not promote invasive cancer (16,53). Indeed, cells with *CDH1* loss are more prone to undergo anoikis (54), a checkpoint whereby cells undergo apoptosis upon loss of attachment (55). *In vivo*, $Cdh1^{-/-}$ gastric epithelial cells were lost over time (16). Cell-cell adhesion (promoted by E-cadherin) suppresses anoikis by activating PI3K/AKT and other pathways (56), a model consistent with our results that pAKT was attenuated in gastric organoids following *Cdh1* inactivation (Fig. 4D). The ability of $RHOA^{Y42C}$ to activate the PI3K pathway may enhance survival and tumorigenicity of *Cdh1*-null gastric cells, via both activation of pAKT and β-catenin. These data suggest that PI3K/AKT inhibition could be used to block Wnt/ β-catenin signaling. However, further studies would be needed to fully evaluate the effects of PI3K/AKT inhibition in DGC given the potential for induction of FOXO3a with these agents to have tumor promoting effects (57). It is notable that the other tumor type associated with germline *CDH1* loss, lobular breast cancer, possesses recurrent co-occurrence of *CDH1* and *PIK3CA* mutations (58). *PIK3CA* mutations are less common in DGC, whereas breast cancers lack recurrent RHO alterations. This unique selection for RHOA dysregulation in DGC suggests the importance of a PI3K- and β-catenin-independent pathway. Additionally, it is the case that not all

RHOA mutant DGCs harbor detectable CDH1 mutations, raising the question of what other alterations may collaborate with RHOA mutation.

Our results showing RHOA/FAK-mediated activation of PI3K and YAP/TAZ could explain the DGC predilection for RHOA mutation. Many studies have implicated RHOA and the actin cytoskeleton as upstream activators of YAP/TAZ (41,42,59). We validated the activation of YAP/TAZ in gastric cells transformed by $RHOA^{Y42C}$ and *Cdh1* loss. Aberrations of the actin cytoskeleton are commonly seen in cancer (60), and enhanced F-actin rearrangement with $RHOA^{Y42C}$ likely provides even greater mechanical stimulus for YAP/TAZ activation. YAP also confers resistance to chemotherapeutic agents in ovarian cancer (61) and oral squamous cell carcinoma (62), suggesting that YAP may contribute to the poor efficacy of cytotoxic therapy in DGC.

Humar *et al.* found that although pFAK was not present in early pre-neoplastic foci in patients with hereditary DGC, FAK became activated in more advanced lesions (53), consistent with our findings that activating FAK with *Cdh1* loss promotes progression. Furthermore, our results establish a contribution of FAK signaling to DGC pathogenesis and demonstrate a mechanistic connection between RHOA and FAK with activation of PI3K/AKT, β-catenin and YAP/TAZ. Whether FAK activation is more ubiquitously essential with CDH1 loss is not established. The sensitivity we observed of DGC cell lines to FAK inhibition implies that FAK may serve as a target for DGCs including those without *RHOA* mutation. Indeed, *CDH1* silencing was shown to sensitize mesothelioma cells to FAK inhibition (63), suggesting a potential role for FAK blockade more broadly in *CDH1*-null cancers.

In summary, these data address uncertainties following discovery of RHOA mutations in DGC. Our biochemical studies establish $RHOA^{Y42C}$ as a gain-of-function mutation that modulates RHOA interaction with downstream effectors. These data demonstrate how aberrant RHOA activation collaborates with loss of tumor suppressor *CDH1* to stimulate signaling networks that mediate transformation (see model, Fig.6O), leading to features typical of the disease, including signet ring cell formation, peritoneal spread and ascites. Furthermore, these models reveal how PI3K activation promotes nuclear β-catenin localization in *CDH1*-null gastric cells by attenuating GSK3β-mediated β-catenin destruction. Our data also demonstrate that FAK activation is a mediator of both PI3K/AKT-β-catenin and YAP activity, secondary to $RHOA^{Y42C}$ mutations. These data and models provide a new foundation for mechanistic and translational inquiry into these deadly cancers where progress has languished, and where treatments continue to be reliant on minimally effective cytotoxic therapy.

METHODS

Generation of Mouse Cohorts

We generated a mouse allele with inducible expression of $RHOA^{Y42C}$. The human *RHOA* cDNA coding region with the Kozak sequence (GCCGCCACC) was introduced into vector pGV at the *EcoRI* cloning site using blunt-end cloning. Sequencing-confirmed pGV-$RHOA^{Y42C}$ vectors were co-electroporated with plasmid expressing FLP recombinase into

mouse ES cells (MESC10, Mirimus) engineered with a FLP homing cassette at *Co1A1* locus, and positive clones were identified by PCR. Positive ES clones were injected into mouse blastocysts for chimera generation. Chimeric mice were crossed with wildtype mice to generate mice with germline mutations. A detailed strategy was previously described (64). The gene is expressed following Cre recombinase-mediated excision of a stop cassette flanked by *LoxP* sites (*loxP*-stop-*loxP* (LSL) *RHOA*$^{Y42C/+}$). *Mist1*-CreERT2, *Cdh1*$^{Flox/Flox}$, *R26*-mTmG mice were developed as previously published (16). *Mist1*-CreERT2, *Cdh1*$^{Flox/Flox}$, *R26*-mTmG mice were crossed with LSL-*RHOA*$^{Y42C/+}$ mice to generate *Mist1*-CreERT2, *Cdh1*$^{Flox/Flox}$, LSL-*RHOA*$^{Y42C/+}$, *R26*-mTmG mice; genotyping was confirmed with appropriate primers (See Supplementary Table S3). All animals were maintained and used in accordance with the guidelines of the Institutional Animal Care and Use Committee of the Dana-Farber Cancer Institute.

Cell Lines

NIH/3T3 mouse fibroblasts were obtained originally from Dr. Geoffrey M. Cooper (Dana-Farber Cancer Institute) and COS-7 cells and HEK293T cells were obtained from ATCC (American Type Culture Collection). Cells were maintained in Dulbecco's Modified Eagle Medium (DMEM) supplemented with 10% calf serum (NIH/3T3) or fetal bovine serum (FBS, COS-7 and HEK293T), penicillin and streptomycin. Cell lines were passaged for one month or 10 passages before a new aliquot was thawed. Cell lines were monitored monthly for mycoplasma contamination using the Lonza MycoAlertTM Mycoplasma Detection Kit and not authenticated. SNU668, NUGC4, AGS and SNU719 were from Broad Institute and maintained in RPMI-1640 supplemented with 10% fetal bovine serum. FU97 was from Broad Institute and maintained in DMEM supplemented with 10% fetal bovine serum and 10 mg/L insulin (Sigma). These cells were authenticated by Broad Institute. Isogenic MCF10 cell lines (CDH1-WT/KO) were purchased from Sigma and maintained in MEGM (Lonza). The isogenic MCF10 cells were authenticated by western blot with E-cadherin antibody. All cell lines were maintained in a humidified chamber with 5% CO_2 at 37°C. Cells were monitored regularly for mycoplasma contamination.

Orthotopic Transplantation

Prior to orthotopic transplantation, organoids were collected and dissociated to approximately single cells using TrypLE Express (Life Technologies). Approximately 5×10^5 cells were resuspended in 50 μl of a mixture of Matrigel and media (1:1). NSG mice (6–8 weeks old, The Jackson Laboratory) were sedated using isoflurane inhalation anesthesia. The stomach was exteriorized through a midline abdominal incision and the 50 μl of cell suspension was surgically injected into the stomach wall with all care to avoiding stomach puncture. The incision was immediately closed using a running 7–0 polypropylene suture (Prolene, Ethicon). The presence of tumors was evaluated by twice weekly abdominal/stomach palpation. All animal experiments were conducted in accordance with protocols approved by the Institutional Animal Care and Use Committee at the Dana-Farber Cancer Institute, in compliance with NIH guidelines.

HPLC GTP Hydrolysis Assay

To measure directly the intrinsic GTP hydrolysis, 70 μM RHOA-GTP was incubated at 25°C in 50 mM HEPES pH 7.5, 100 mM NaCl, 5 mM $MgCl_2$, 5% glycerol and 5 mM β-mercaptoethanol. Aliquots of 40 μl were flash frozen in liquid nitrogen at indicated time points to stop the reaction and incubated for 2 min at 95°C. After centrifugation (14,000 x g, 1 min) of the denatured protein, the supernatant was applied to a high-performance liquid chromatography column (HPLC, Agilent 1100). GDP and GTP were separated on a C18-column (Agilent) with 100 mM potassium-phosphate pH 6.5, 10 mM tert-butyl-ammonium-bromide and 7.5% acetonitrile as mobile phase (65). The concentration of non-hydrolyzed GTP was plotted against time. Data were described by a mono-exponential equation to determine the observed rate constant (k_{obs}) using GraphPad Prism. A similar protocol was used to measure the efficiency of RHOA nucleotide loading (25% acetonitrile for mant-nucleotides).

Chemicals and Drugs

See Supplementary Table S4.

Antibodies

See Supplementary Table S5.

Reverse Phase Protein Microarray (RPPA)

RPPA analysis was performed in triplicate on gastric organoids harboring various *Cdh1* and *RHOA* genetic perturbations. Samples were lysed as previously described (66). Cell lysates from organoids were immobilized onto nitrocellulose-coated glass slides (Grace Bio-labs) using an Aushon 2470 arrayer (Aushon BioSystems) in biological triplicates along with reference standards for quality control. Selected arrays were stained with Sypro Ruby Protein Blot Stain following manufacturer's instructions to quantify the amount of protein in each sample. Immunostaining was performed as previously described (66). Clustering by antibodies was performed using k-means clustering. Fold change values represented were calculated with respect to the corresponding RHOA-EV control median intensity value by *Cdh1* status and subsequently log2 changed, unless otherwise noted. Testing between specific comparisons utilized the Student's T-test with p-values < 0.05 denoting significant alterations. Testing results were represented by volcano plots and/or reported in supplementary tables. Heatmaps were generated in R using the ComplexHeatmap package from Bioconductor.

Live-cell Confocal Imaging

Mouse organoids expressing GFP (*R26-mTmG* after tamoxifen induction) were cultured in conditioned media in a Lab-Tek II Chambered Coverglass system dish. Images of organoids with different genotypes were captured on an LSM 510 Meta live-cell confocal microscope, with GFP autofluorescence images taken every ten min for a total of 36–48 h of culture. For PF-573228 treatment, $Cdh1^{-/-}RHOA^{Y42C/+}$GFP organoids were collected and dissociated into single cells using TrypLE Express, then plated into the same coverglass system at a density of 40,000 cells/25 μL Matrigel, and cultured for 2 days prior to treatment with

DMSO or PF-573228 (5 μM). Live-cell imaging was started immediately after drug treatment.

Statistical Analysis

Data are represented as mean ± S.D. or S.E.M. as indicated in the figure legends. For each experiment, the number of independent biological experiments are as noted in the figure legends, with representative images shown of replicates with similar results. Statistical analysis was performed using Microsoft Office statistical tools or in Prism 7.0 (GraphPad). Pairwise comparisons between groups (that is, experimental versus control) were performed using an unpaired two-tailed Student's *t*-test, one-way ANOVA Tukey's multiple comparison test, or two-way ANOVA as appropriate. $P < 0.05$ is considered to be statistically significant. P-values are denoted by $*P < 0.05$, $**P < 0.01$, $** P < 0.001$, $****P < 0.0001$. For all experiments, the variance between comparison groups was found to be equivalent. Sample sizes and animal numbers were determined from pilot laboratory experiments and previously published literature. Animals were excluded from analysis if they were euthanized due to health reasons unrelated to tumor growth. For *in vivo* experiments, all mice were randomized before drug treatment.

Supplementary Material

Refer to Web version on PubMed Central for supplementary material.

Acknowledgments

Financial support: This work was supported by grants from the National Cancer Institute (NCI) (R01 CA223775 to A.J.Bass, C.J.Der and T.C.Wang), The DeGregorio Family Foundation (A.J.Bass and T.C.Wang) and the Department of Defense Congressional Directed Medical Research Program (H.Zhang). H.Zhang was supported by the 2017 Debbie's Dream Foundation-AACR Gastric Cancer Research Fellowship, Grant Number 17-40-41-ZHAN. R.G.Hodge was supported by the 2018 Debbie's Dream Foundation-AACR Gastric Cancer Research Fellowship, in Memory of Sally Mandel, Grant Number 18-40-41-HODG. D.R.Blake was supported by NCI fellowships (T32CA071341 and F31CA216965). J.N. Diehl was supported by NCI T32CA071341 and the Slomo and Cindy Silvian Foundation. A.J.Bass received support from a DFCI Medical Oncology pilot project grant and the Schottenstein Gastric Cancer Fund. Histology and confocal core services were supported by the Harvard Digestive Disease Center and NIH grant P30DK034854.

Disclosure of Potential Conflicts of Interest

A.J.Bass receives research funding from Merck, Bayer and Novartis, and is a consultant to Earli, Glenmark and HelixNano. A.J.Bass and H.Zhang are Co-Founders of Signet Therapeutics. K.K.Wong is a founder and equity holder of G1 Therapeutics and he has consulting/sponsored research agreements with MedImmune, Takeda, TargImmune, BMS, AstraZeneca, Janssen, Pfizer, Novartis, Merck, Ono, and Array. C.J.Der is on the scientific advisory board of Mirati Therapeutics, is a consultant for Deciphera Pharmaceuticals, Ribometrix and Eli Llly, and receives research funding from Mirati Therapeutics and Deciphera Pharmaceuticals. G.Church's disclosures: v.ht/PHNc.

REFERENCES

1. Ferlay J, Soerjomataram I, Dikshit R, Eser S, Mathers C, Rebelo M, et al. Cancer incidence and mortality worldwide: sources, methods and major patterns in GLOBOCAN 2012. Int J Cancer 2015;136(5):E359–86 doi 10.1002/ijc.29210. [PubMed: 25220842]
2. Lauren P The Two Histological Main Types of Gastric Carcinoma: Diffuse and So-Called Intestinal-Type Carcinoma. An Attempt at a Histo-Clinical Classification. Acta Pathol Microbiol Scand 1965;64:31–49. [PubMed: 14320675]

3. Kakiuchi M, Nishizawa T, Ueda H, Gotoh K, Tanaka A, Hayashi A, et al. Recurrent gain-of-function mutations of RHOA in diffuse-type gastric carcinoma. Nat Genet 2014;46(6):583–7 doi 10.1038/ng.2984. [PubMed: 24816255]
4. Cancer Genome Atlas Research N. Comprehensive molecular characterization of gastric adenocarcinoma. Nature 2014;513(7517):202–9 doi 10.1038/nature13480. [PubMed: 25079317]
5. Becker KF, Atkinson MJ, Reich U, Becker I, Nekarda H, Siewert JR, et al. E-cadherin gene mutations provide clues to diffuse type gastric carcinomas. Cancer Res 1994;54(14):3845–52. [PubMed: 8033105]
6. Tamura G, Yin J, Wang S, Fleisher AS, Zou T, Abraham JM, et al. E-Cadherin gene promoter hypermethylation in primary human gastric carcinomas. J Natl Cancer Inst 2000;92(7):569–73. [PubMed: 10749913]
7. Rashid H, Alam K, Afroze D, Yousuf A, Banday M, Kawoosa F. Hypermethylation Status of E-Cadherin Gene in Gastric Cancer Patients in a High Incidence Area. Asian Pac J Cancer Prev 2016;17(6):2757–60. [PubMed: 27356686]
8. Richards FM, McKee SA, Rajpar MH, Cole TR, Evans DG, Jankowski JA, et al. Germline E-cadherin gene (CDH1) mutations predispose to familial gastric cancer and colorectal cancer. Hum Mol Genet 1999;8(4):607–10. [PubMed: 10072428]
9. Guilford P, Hopkins J, Harraway J, McLeod M, McLeod N, Harawira P, et al. E-cadherin germline mutations in familial gastric cancer. Nature 1998;392(6674):402–5 doi 10.1038/32918. [PubMed: 9537325]
10. Wang K, Yuen ST, Xu J, Lee SP, Yan HH, Shi ST, et al. Whole-genome sequencing and comprehensive molecular profiling identify new driver mutations in gastric cancer. Nat Genet 2014;46(6):573–82 doi 10.1038/ng.2983. [PubMed: 24816253]
11. Mun DG, Bhin J, Kim S, Kim H, Jung JH, Jung Y, et al. Proteogenomic Characterization of Human Early-Onset Gastric Cancer. Cancer Cell 2019;35(1):111–24 e10 doi 10.1016/j.ccell.2018.12.003. [PubMed: 30645970]
12. Yan HHN, Siu HC, Law S, Ho SL, Yue SSK, Tsui WY, et al. A Comprehensive Human Gastric Cancer Organoid Biobank Captures Tumor Subtype Heterogeneity and Enables Therapeutic Screening. Cell Stem Cell 2018;23(6):882–97 e11 doi 10.1016/j.stem.2018.09.016. [PubMed: 30344100]
13. Hodge RG, Ridley AJ. Regulating Rho GTPases and their regulators. Nat Rev Mol Cell Biol 2016;17(8):496–510 doi 10.1038/nrm.2016.67. [PubMed: 27301673]
14. Stange DE, Koo BK, Huch M, Sibbel G, Basak O, Lyubimova A, et al. Differentiated Troy(+) Chief Cells Act as Reserve Stem Cells to Generate All Lineages of the Stomach Epithelium. Cell 2013;155(2):357–68 doi 10.1016/j.cell.2013.09.008. [PubMed: 24120136]
15. Nam KT, Lee HJ, Sousa JF, Weis VG, O'Neal RL, Finke PE, et al. Mature Chief Cells Are Cryptic Progenitors for Metaplasia in the Stomach. Gastroenterology 2010;139(6):2028–U324 doi 10.1053/j.gastro.2010.09.005. [PubMed: 20854822]
16. Hayakawa Y, Ariyama H, Stancikova J, Sakitani K, Asfaha S, Renz BW, et al. Mist1 Expressing Gastric Stem Cells Maintain the Normal and Neoplastic Gastric Epithelium and Are Supported by a Perivascular Stem Cell Niche. Cancer Cell 2015;28(6):800–14 doi 10.1016/j.ccell.2015.10.003. [PubMed: 26585400]
17. Nanki K, Toshimitsu K, Takano A, Fujii M, Shimokawa M, Ohta Y, et al. Divergent Routes toward Wnt and R-spondin Niche Independency during Human Gastric Carcinogenesis. Cell 2018;174(4):856–69 e17 doi 10.1016/j.cell.2018.07.027. [PubMed: 30096312]
18. Paterson HF, Self AJ, Garrett MD, Just I, Aktories K, Hall A. Microinjection of recombinant p21rho induces rapid changes in cell morphology. J Cell Biol 1990;111(3):1001–7. [PubMed: 2118140]
19. Ridley AJ, Hall A. The small GTP-binding protein rho regulates the assembly of focal adhesions and actin stress fibers in response to growth factors. Cell 1992;70(3):389–99. [PubMed: 1643657]
20. Khosravi-Far R, Chrzanowska-Wodnicka M, Solski PA, Eva A, Burridge K, Der CJ. Dbl and Vav mediate transformation via mitogen-activated protein kinase pathways that are distinct from those activated by oncogenic Ras. Mol Cell Biol 1994;14(10):6848–57. [PubMed: 7935402]

21. Ren XD, Kiosses WB, Schwartz MA. Regulation of the small GTP-binding protein Rho by cell adhesion and the cytoskeleton. EMBO J 1999;18(3):578–85 doi 10.1093/emboj/18.3.578. [PubMed: 9927417]
22. Warner H, Wilson BJ, Caswell PT. Control of adhesion and protrusion in cell migration by Rho GTPases. Curr Opin Cell Biol 2018;56:64–70 doi 10.1016/j.ceb.2018.09.003. [PubMed: 30292078]
23. Olivo C, Vanni C, Mancini P, Silengo L, Torrisi MR, Tarone G, et al. Distinct involvement of cdc42 and RhoA GTPases in actin organization and cell shape in untransformed and Dbl oncogene transformed NIH3T3 cells. Oncogene 2000;19(11):1428–36 doi 10.1038/sj.onc.1203440. [PubMed: 10723134]
24. Zhang ZG, Lambert CA, Servotte S, Chometon G, Eckes B, Krieg T, et al. Effects of constitutively active GTPases on fibroblast behavior. Cell Mol Life Sci 2006;63(1):82–91 doi 10.1007/s00018-005-5416-5. [PubMed: 16378244]
25. Singh A, Karnoub AE, Palmby TR, Lengyel E, Sondek J, Der CJ. Rac1b, a tumor associated, constitutively active Rac1 splice variant, promotes cellular transformation. Oncogene 2004;23(58):9369–80 doi 10.1038/sj.onc.1208182. [PubMed: 15516977]
26. Rolli-Derkinderen M, Sauzeau V, Boyer L, Lemichez E, Baron C, Henrion D, et al. Phosphorylation of serine 188 protects RhoA from ubiquitin/proteasome-mediated degradation in vascular smooth muscle cells. Circ Res 2005;96(11):1152–60 doi 10.1161/01.RES.0000170084.88780.ea. [PubMed: 15890975]
27. Strassheim D, Porter RA, Phelps SH, Williams CL. Unique in vivo associations with SmgGDS and RhoGDI and different guanine nucleotide exchange activities exhibited by RhoA, dominant negative RhoA(Asn-19), and activated RhoA(Val-14). J Biol Chem 2000;275(10):6699–702. [PubMed: 10702222]
28. Davis MJ, Ha BH, Holman EC, Halaban R, Schlessinger J, Boggon TJ. RAC1P29S is a spontaneously activating cancer-associated GTPase. Proc Natl Acad Sci U S A 2013;110(3):912–7 doi 10.1073/pnas.1220895110. [PubMed: 23284172]
29. Jin Y, Yu Y, Shao Q, Ma Y, Zhang R, Yao H, et al. Up-regulation of ECT2 is associated with poor prognosis in gastric cancer patients. Int J Clin Exp Pathol 2014;7(12):8724–31. [PubMed: 25674238]
30. Jaiswal M, Dvorsky R, Ahmadian MR. Deciphering the molecular and functional basis of Dbl family proteins: a novel systematic approach toward classification of selective activation of the Rho family proteins. J Biol Chem 2013;288(6):4486–500 doi 10.1074/jbc.M112.429746. [PubMed: 23255595]
31. Sahai E, Alberts AS, Treisman R. RhoA effector mutants reveal distinct effector pathways for cytoskeletal reorganization, SRF activation and transformation. EMBO J 1998;17(5):1350–61 doi 10.1093/emboj/17.5.1350. [PubMed: 9482732]
32. Zohar M, Teramoto H, Katz BZ, Yamada KM, Gutkind JS. Effector domain mutants of Rho dissociate cytoskeletal changes from nuclear signaling and cellular transformation. Oncogene 1998;17(8):991–8 doi 10.1038/sj.onc.1202022. [PubMed: 9747878]
33. Watanabe N, Kato T, Fujita A, Ishizaki T, Narumiya S. Cooperation between mDia1 and ROCK in Rho-induced actin reorganization. Nat Cell Biol 1999;1(3):136–43 doi 10.1038/11056. [PubMed: 10559899]
34. Blumenstein L, Ahmadian MR. Models of the cooperative mechanism for Rho effector recognition: implications for RhoA-mediated effector activation. J Biol Chem 2004;279(51):53419–26 doi 10.1074/jbc.M409551200. [PubMed: 15475352]
35. Rose R, Weyand M, Lammers M, Ishizaki T, Ahmadian MR, Wittinghofer A. Structural and mechanistic insights into the interaction between Rho and mammalian Dia. Nature 2005;435(7041):513–8 doi 10.1038/nature03604. [PubMed: 15864301]
36. Chen M, Bresnick AR, O'Connor KL. Coupling S100A4 to Rhotekin alters Rho signaling output in breast cancer cells. Oncogene 2013;32(32):3754–64 doi 10.1038/onc.2012.383. [PubMed: 22964635]

37. Amano M, Chihara K, Kimura K, Fukata Y, Nakamura N, Matsuura Y, et al. Formation of actin stress fibers and focal adhesions enhanced by Rho-kinase. Science 1997;275(5304):1308–11. [PubMed: 9036856]
38. Wu D, Pan W. GSK3: a multifaceted kinase in Wnt signaling. Trends Biochem Sci 2010;35(3): 161–8 doi 10.1016/j.tibs.2009.10.002. [PubMed: 19884009]
39. Rubinfeld B, Albert I, Porfiri E, Fiol C, Munemitsu S, Polakis P. Binding of GSK3beta to the APC-beta-catenin complex and regulation of complex assembly. Science 1996;272(5264):1023–6. [PubMed: 8638126]
40. Beurel E, Grieco SF, Jope RS. Glycogen synthase kinase-3 (GSK3): regulation, actions, and diseases. Pharmacol Ther 2015;148:114–31 doi 10.1016/j.pharmthera.2014.11.016. [PubMed: 25435019]
41. Park HW, Kim YC, Yu B, Moroishi T, Mo JS, Plouffe SW, et al. Alternative Wnt Signaling Activates YAP/TAZ. Cell 2015;162(4):780–94 doi 10.1016/j.cell.2015.07.013. [PubMed: 26276632]
42. Wang L, Luo JY, Li B, Tian XY, Chen LJ, Huang Y, et al. Integrin-YAP/TAZ-JNK cascade mediates atheroprotective effect of unidirectional shear flow. Nature 2016;540(7634):579–82 doi 10.1038/nature20602. [PubMed: 27926730]
43. Rosenbluh J, Nijhawan D, Cox AG, Li X, Neal JT, Schafer EJ, et al. beta-Catenin-driven cancers require a YAP1 transcriptional complex for survival and tumorigenesis. Cell 2012;151(7):1457–73 doi 10.1016/j.cell.2012.11.026. [PubMed: 23245941]
44. Wong GS, Zhou J, Liu JB, Wu Z, Xu X, Li T, et al. Targeting wild-type KRAS-amplified gastroesophageal cancer through combined MEK and SHP2 inhibition. Nat Med 2018;24(7):968–77 doi 10.1038/s41591-018-0022-x. [PubMed: 29808010]
45. Konstantinidou G, Ramadori G, Torti F, Kangasniemi K, Ramirez RE, Cai Y, et al. RHOA-FAK is a required signaling axis for the maintenance of KRAS-driven lung adenocarcinomas. Cancer Discov 2013;3(4):444–57 doi 10.1158/2159-8290.CD-12-0388. [PubMed: 23358651]
46. Sulzmaier FJ, Jean C, Schlaepfer DD. FAK in cancer: mechanistic findings and clinical applications. Nat Rev Cancer 2014;14(9):598–610 doi 10.1038/nrc3792. [PubMed: 25098269]
47. Ge S, Xia X, Ding C, Zhen B, Zhou Q, Feng J, et al. A proteomic landscape of diffuse-type gastric cancer. Nat Commun 2018;9(1):1012 doi 10.1038/s41467-018-03121-2. [PubMed: 29520031]
48. Mulligan LM. RET revisited: expanding the oncogenic portfolio. Nat Rev Cancer 2014;14(3):173–86 doi 10.1038/nrc3680. [PubMed: 24561444]
49. Yoon C, Cho SJ, Aksoy BA, Park DJ, Schultz N, Ryeom SW, et al. Chemotherapy Resistance in Diffuse-Type Gastric Adenocarcinoma Is Mediated by RhoA Activation in Cancer Stem-Like Cells. Clin Cancer Res 2016;22(4):971–83 doi 10.1158/1078-0432.CCR-15-1356. [PubMed: 26482039]
50. Yao F, Kausalya JP, Sia YY, Teo AS, Lee WH, Ong AG, et al. Recurrent Fusion Genes in Gastric Cancer: CLDN18-ARHGAP26 Induces Loss of Epithelial Integrity. Cell Rep 2015;12(2):272–85 doi 10.1016/j.celrep.2015.06.020. [PubMed: 26146084]
51. Shu Y, Zhang W, Hou Q, Zhao L, Zhang S, Zhou J, et al. Prognostic significance of frequent CLDN18-ARHGAP26/6 fusion in gastric signet-ring cell cancer. Nat Commun 2018;9(1):2447 doi 10.1038/s41467-018-04907-0. [PubMed: 29961079]
52. Khosravi-Far R, White MA, Westwick JK, Solski PA, Chrzanowska-Wodnicka M, Van Aelst L, et al. Oncogenic Ras activation of Raf/mitogen-activated protein kinase-independent pathways is sufficient to cause tumorigenic transformation. Mol Cell Biol 1996;16(7):3923–33. [PubMed: 8668210]
53. Humar B, Fukuzawa R, Blair V, Dunbier A, More H, Charlton A, et al. Destabilized adhesion in the gastric proliferative zone and c-Src kinase activation mark the development of early diffuse gastric cancer. Cancer Res 2007;67(6):2480–9 doi 10.1158/0008-5472.CAN-06-3021. [PubMed: 17363565]
54. Butler DE, Marlein C, Walker HF, Frame FM, Mann VM, Simms MS, et al. Inhibition of the PI3K/AKT/mTOR pathway activates autophagy and compensatory Ras/Raf/MEK/ERK signalling in prostate cancer. Oncotarget 2017;8(34):56698–713 doi 10.18632/oncotarget.18082. [PubMed: 28915623]

55. Paoli P, Giannoni E, Chiarugi P. Anoikis molecular pathways and its role in cancer progression. Biochim Biophys Acta 2013;1833(12):3481–98 doi 10.1016/j.bbamcr.2013.06.026. [PubMed: 23830918]
56. Grossmann J Molecular mechanisms of "detachment-induced apoptosis--Anoikis". Apoptosis 2002;7(3):247–60. [PubMed: 11997669]
57. Tenbaum SP, Ordonez-Moran P, Puig I, Chicote I, Arques O, Landolfi S, et al. beta-catenin confers resistance to PI3K and AKT inhibitors and subverts FOXO3a to promote metastasis in colon cancer. Nat Med 2012;18(6):892–901 doi 10.1038/nm.2772. [PubMed: 22610277]
58. Ciriello G, Gatza ML, Beck AH, Wilkerson MD, Rhie SK, Pastore A, et al. Comprehensive Molecular Portraits of Invasive Lobular Breast Cancer. Cell 2015;163(2):506–19 doi 10.1016/j.cell.2015.09.033. [PubMed: 26451490]
59. Yu FX, Zhao B, Guan KL. Hippo Pathway in Organ Size Control, Tissue Homeostasis, and Cancer. Cell 2015;163(4):811–28 doi 10.1016/j.cell.2015.10.044.
60. Olson MF, Sahai E. The actin cytoskeleton in cancer cell motility. Clin Exp Metastasis 2009;26(4):273–87 doi 10.1007/s10585-008-9174-2. [PubMed: 18498004]
61. Zhang X, George J, Deb S, Degoutin JL, Takano EA, Fox SB, et al. The Hippo pathway transcriptional co-activator, YAP, is an ovarian cancer oncogene. Oncogene 2011;30(25):2810–22 doi 10.1038/onc.2011.8. [PubMed: 21317925]
62. Yoshikawa K, Noguchi K, Nakano Y, Yamamura M, Takaoka K, Hashimoto-Tamaoki T, et al. The Hippo pathway transcriptional co-activator, YAP, confers resistance to cisplatin in human oral squamous cell carcinoma. Int J Oncol 2015;46(6):2364–70 doi 10.3892/ijo.2015.2948. [PubMed: 25846049]
63. Kato T, Sato T, Yokoi K, Sekido Y. E-cadherin expression is correlated with focal adhesion kinase inhibitor resistance in Merlin-negative malignant mesothelioma cells. Oncogene 2017;36(39):5522–31 doi 10.1038/onc.2017.147. [PubMed: 28553954]
64. Akbay EA, Moslehi J, Christensen CL, Saha S, Tchaicha JH, Ramkissoon SH, et al. D-2-hydroxyglutarate produced by mutant IDH2 causes cardiomyopathy and neurodegeneration in mice. Genes Dev 2014;28(5):479–90 doi 10.1101/gad.231233.113. [PubMed: 24589777]
65. Schaefer A, Miertzschke M, Berken A, Wittinghofer A. Dimeric plant RhoGAPs are regulated by its CRIB effector motif to stimulate a sequential GTP hydrolysis. J Mol Biol 2011;411(4):808–22 doi 10.1016/j.jmb.2011.06.033. [PubMed: 21723292]
66. Baldelli E, Calvert V, Hodge A, VanMeter A, Petricoin EF 3rd, Pierobon M Reverse Phase Protein Microarrays. Methods Mol Biol 2017;1606:149–69 doi 10.1007/978-1-4939-6990-6_11. [PubMed: 28502000]

SIGNIFICANCE

The functional significance of recurrent RHOA mutations in DGC has remained unresolved. Through biochemical studies and mouse modeling of the hotspot $RHOA^{Y42C}$ mutation we establish that these mutations are activating, detail their effects upon cell signaling and define how RHOA-mediated FAK activation imparts sensitivity to pharmacologic FAK inhibitors.

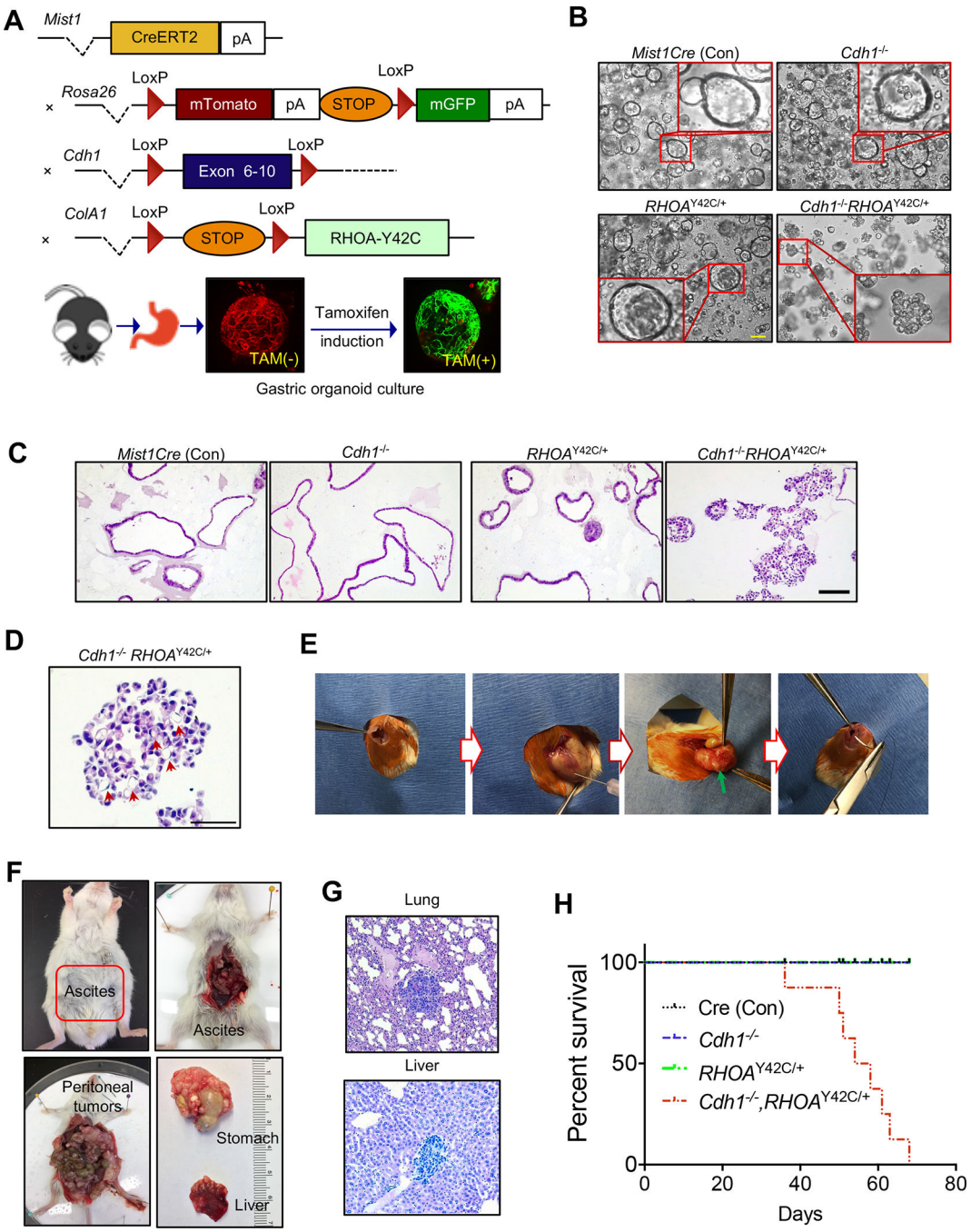

Figure 1. *Cdh1* loss with *RHOA* hotspot mutation induces diffuse gastric cancer *in vivo*.

A, Schematic for the generation of mice with distinct genotypes, including the tomato-GFP reporter allele; bottom: representative stack confocal image of gastric organoids with *Mist1*CreERT2-R26mTmG 48 hours after tamoxifen (2 μM) induction *in vitro*. Representative images of (**B**) phase contrast and (**C**) H&E for gastric organoids with annotated genotypes after three weeks following *in vitro* tamoxifen induction. Scale bar = 100 μm. **D,** Representative higher-magnification image showing signet ring cells in $Cdh1^{-/-}RHOA^{Y42C/+}$organoids following tamoxifen induction. Scale bar = 50 μm. **E,**

Procedure of orthotopic injection into gastric wall with green arrow noting location following injection. **F,** Representative gross images of mouse with gastric tumor, ascites, peritoneal spread with liver metastases at eight weeks following orthotopic injection of *Cdh1*$^{-/-}$*RHOA*$^{Y42C/+}$ organoids. **G,** Representative H&E images of liver and lung metastases following orthotopic implantation of *Cdh1*$^{-/-}$*RHOA*$^{Y42C/+}$ organoids. Scale bar = 100 μm. **H,** Kaplan-Meier survival curve following orthotopic implantation of organoids of noted genotypes. Log-rank (Mantel-Cox) test, P=0.0047 (*Cdh1*$^{-/-}$*RHOA*$^{Y42C/+}$ versus other genotypes).

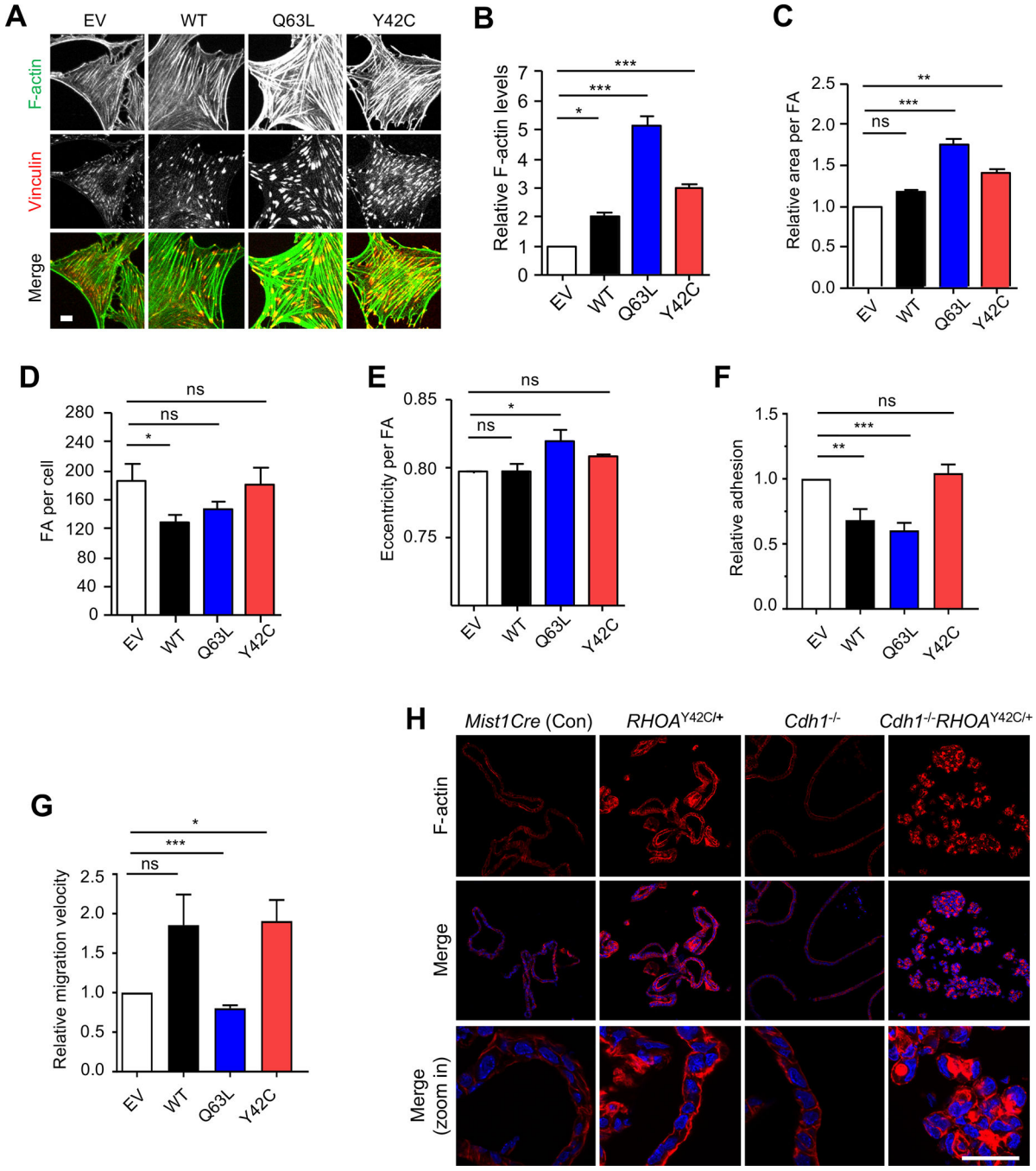

Figure 2. RHOA^{Y42C} is a mutation with gain-of-function by stimulating stress fibers and focal adhesions.

A, Immunofluorescence analysis of NIH/3T3 fibroblasts stably expressing exogenous HA epitope-tagged RHOA WT and mutant proteins, stained with phalloidin to monitor stress fiber formation and anti-vinculin antibody to visualize focal adhesions (FA). Images are representative of three independent experiments. Scale bar = 10 μm. **B,** Quantitation of stress fiber formation in the cells from (**A**), by calculating the corrected total cell fluorescence (20 cells per condition, n = 3 independent experiments). To measure FA assembly in the cells

from (**A**), the area of each FA (**C**), the number of FA per cell (**D**), and the eccentricity of each FA (**E**) was calculated based on the vinculin staining (1307 to 2295 FA in 14 to 20 cells per condition, n = 3). Data are mean ± S.E.M. **F,** CMFDA-labelled NIH/3T3 cells were allowed to adhere upon fibronectin for 1 h. Data are mean ± S.E.M. (n = 3). **G,** Images of cells during random migration were captured using a time lapse microscope at 1 frame/10 min for 16 h. Data are mean migration velocities ± S.E.M. (n = 4, 25 cells per experiment); ***P<0.001, **P<0.01, *P<0.05, ns, not significant; P values from one-way ANOVA with Tukey's multiple comparison test. **H,** Representative immunofluorescence images for F-actin in organoids from mice with annotated genotypes. Phalloidin (in red) was used to visualize F-actin, DAPI (in blue) for the nucleus. Scale bar = 50 μm.

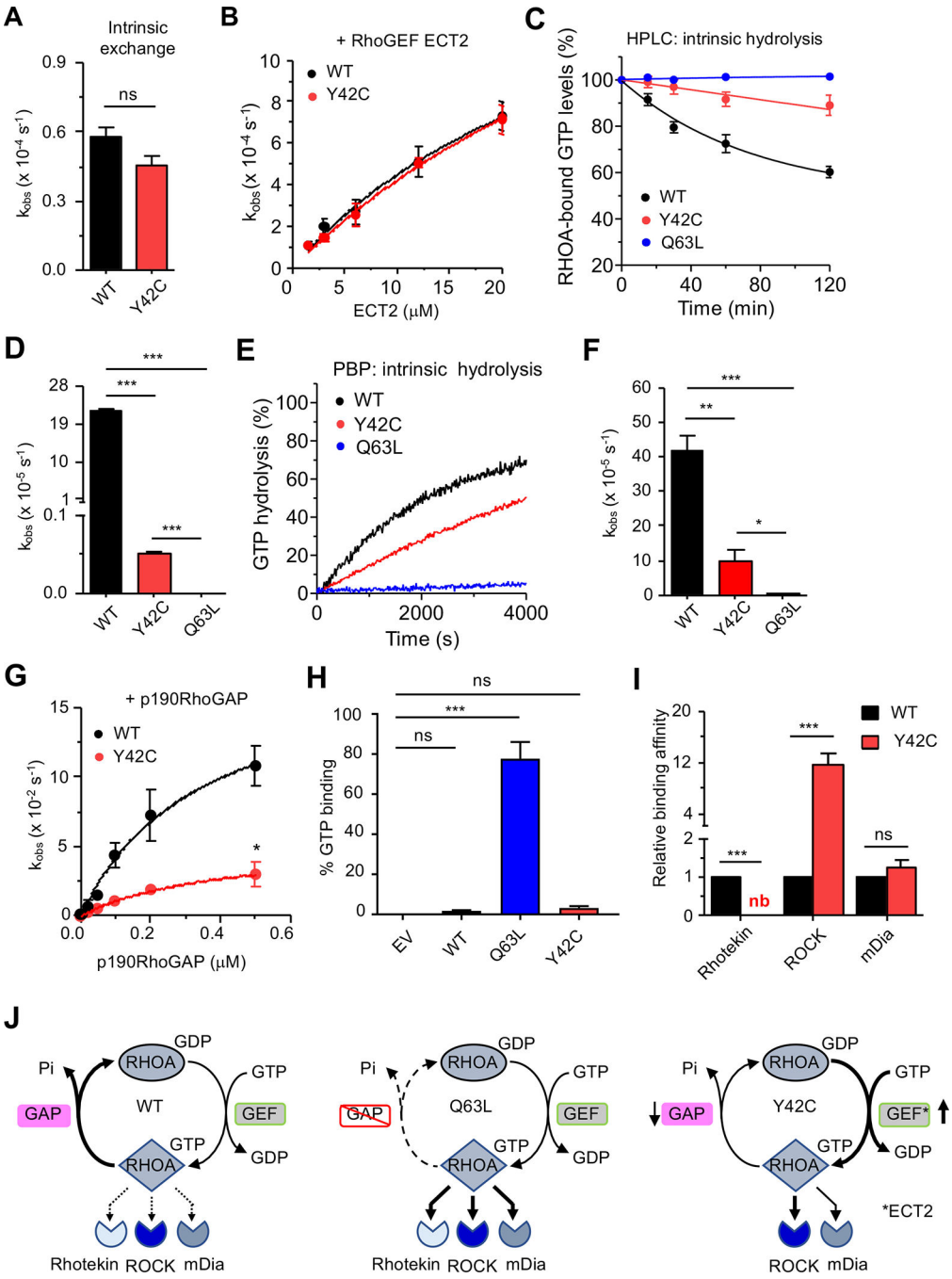

Figure 3. RHOA^{Y42C} exhibits impaired GTP hydrolysis and altered effector binding.

A, *E. coli*-expressed RHOA proteins were evaluated *in vitro*. Intrinsic guanine nucleotide exchange activity (n = 3). **B,** Recombinant ECT2 DH-PH catalytic domain stimulation of RHOA nucleotide exchange activity (n = 3). Intrinsic RHOA GTP hydrolysis activity was determined by (**C, D**) directly measuring RHOA bound GTP levels (n = 4) or (**E, F**) based on phosphate release using the phosphate binding protein sensor (n = 2). **G,** Determination of p190RhoGAP catalytic domain stimulation of RHOA GTP hydrolysis activity using the phosphate binding protein sensor (n = 2). Data in A-G are mean ± S.E.M.; ***P<0.001,

** $P<0.01$, * $P<0.05$, ns, not significant; unpaired *t*-test. **H,** RHOA guanine nucleotide binding was determined in NIH/3T3 cells expressing the indicated RHOA proteins by ^{32}P-metabolic labeling (n = 2). Data are mean ± S.E.M., *** $P<0.001$, ns, not significant; one-way ANOVA with Tukey's multiple comparison test. **I,** Normalized binding affinities of RHOA WT and Y42C to RBD domains of indicated effectors, as determined in effector-nucleotide dissociation assays; nb = binding too weak to be detected (n = 3). All affinities were normalized to RHOA WT binding to each effector. Data are mean ± S.E.M.; *** $P<0.001$, ns, not significant; unpaired *t*-test. **J,** Comparison of WT and mutant RHOA biochemical properties.

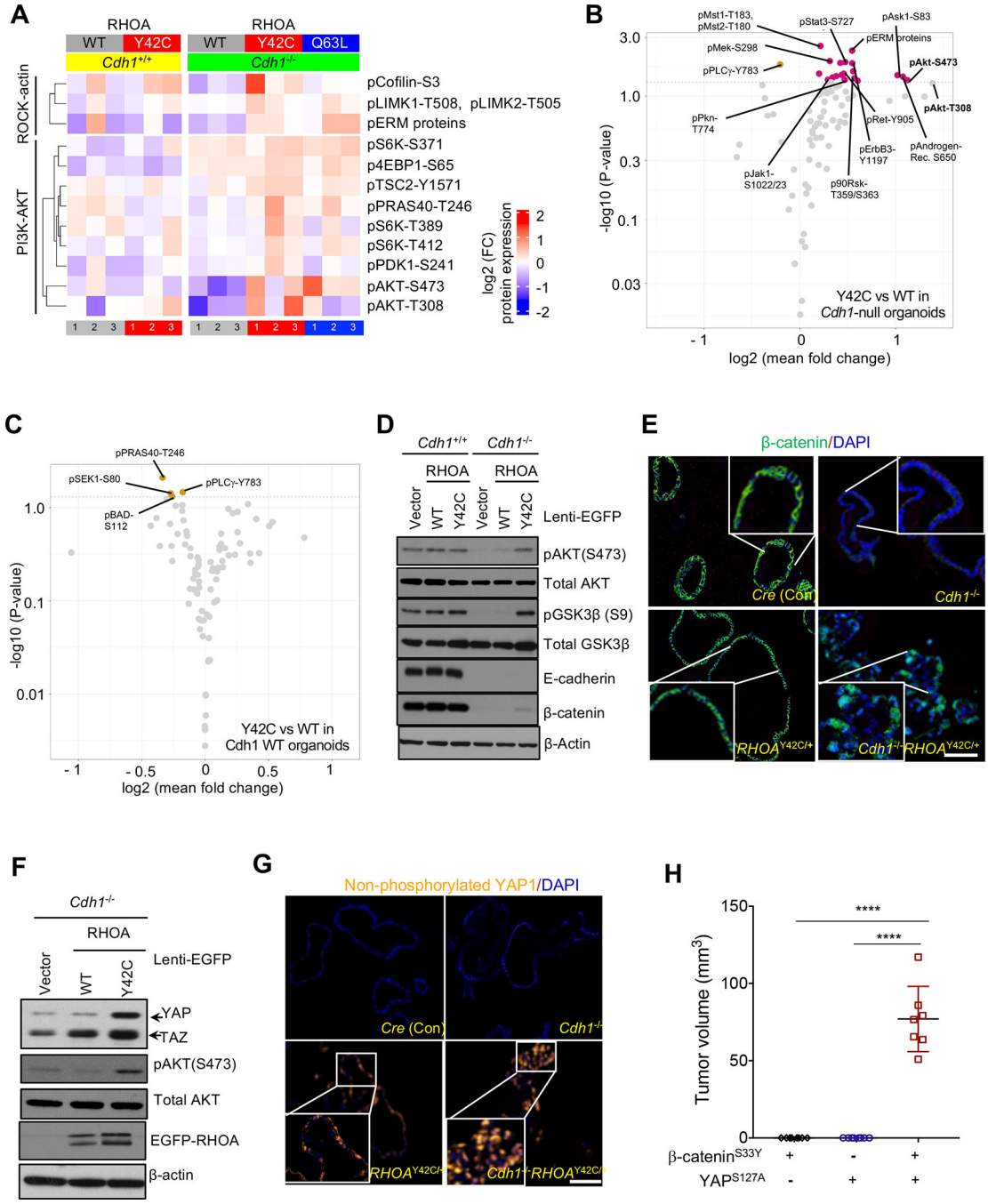

Figure 4. RHOA^{Y42C} promotes activation of PI3K/β-catenin and YAP/TAZ.

A, Heatmap representation of selected antibodies from RPPA analysis of isogenic gastric organoids with annotated genotypes. *Cdh1*$^{+/+}$ and *Cdh1*$^{-/-}$ fold change values were calculated with respect to matched RHOA-EV controls per antibody (see also Supplementary Fig. S4A, S4D, S4E and Supplementary Table S1). Resulting values were log2 changed and clustered using k-means clustering for antibodies. **B-C,** Volcano plots representing results comparing RHOA^{Y42C} versus RHOA^{WT} in (**B**) *Cdh1*-null organoids or (**C**) in *Cdh1* WT organoids by RPPA analysis. Significantly upregulated and downregulated

proteins and phosphorylation sites are represented by pink and gold dots, respectively. Horizontal dotted line represents p-value threshold of 0.05. The list of top protein phosphorylation/expression differences is provided in Supplementary Table S1. **D,** Immunoblots of *Cdh1* intact and null isogenic organoids engineered with lentiviral EGFP-RHOA^{Y42C} or controls (representative image from 3 independent experiments). **E,** Immunofluorescence analysis of β-catenin in organoids from mice with annotated genomes. Scale bar = 100 μm. **F,** Immunoblotting for YAP in *Cdh1*-null organoids with lentiviral EGFP-RHOA^{Y42C} or controls (representative image from 3 independent experiments). **G,** Immunofluorescence of active (non-phosphorylated) YAP in organoids from mice of annotated genomes. Scale bar = 100 μm. **H,** Tumor incidence of *Cdh1*-null organoids with ectopic expression of YAP(S127A) or β-catenin(S33Y) or both vectors, implanted into flanks of NSG mice. Data are mean ± S.D; ****P<0.0001, unpaired two-tailed Student's t-test.

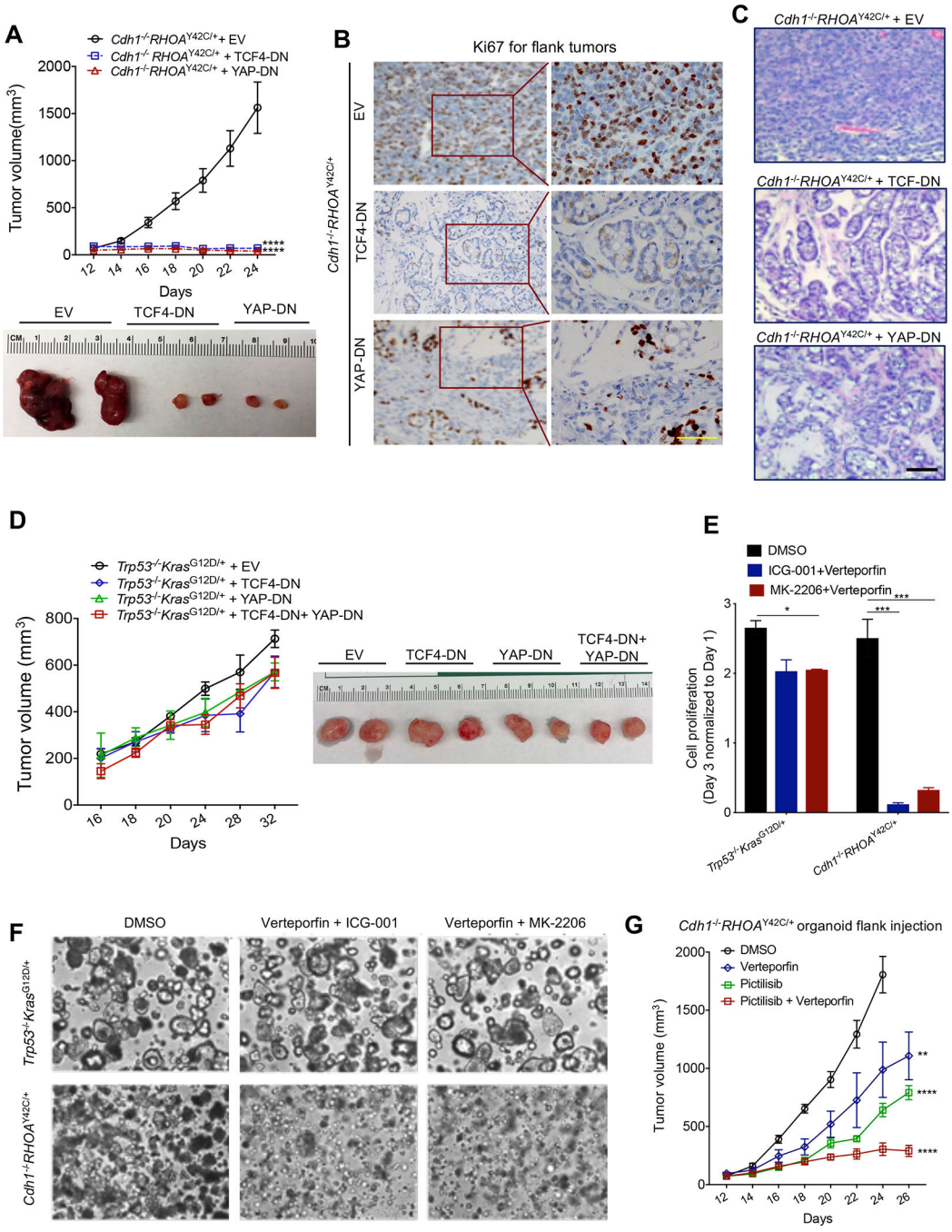

Figure 5. YAP and β-catenin pathways are both required for the *Cdh1*$^{-/-}$*RHOA*$^{Y42C/+}$-induced transformation.

A, Tumor volume of *Cdh1*$^{-/-}$*RHOA*$^{Y42C/+}$ organoids with ectopic expression of either TCF4-DN (del aa 1–31) or YAP-DN (S94A) followed by flank implantation, with representative images (bottom) of tumors from each group (n=4 for each). Data are mean ± S.E.M. ****P<0.0001, two-way ANOVA, (TCF4-DN or YAP-DN versus EV group). **B,** Representative images of Ki67 staining of the tumors from (**A**). Scale bar = 50 μm. **C,** Representative H&E images for the tumors from (**A**). Scale bar = 100 μm. **D,** Tumor volume

of *Trp53*$^{-/-}$*Kras*$^{G12D/+}$ organoids with ectopic expression of TCF4-DN (del aa 1–31) or YAP-DN (S94A) or combination, implanted into flanks, with representative images of tumors from each group (n = 4 for each). Data are mean ± S.E.M. **E,** *In vitro* proliferation of *Cdh1*$^{-/-}$*RHOA*$^{Y42C/+}$ and *Trp53*$^{-/-}$*Kras*$^{G12D/+}$ organoids treated with DMSO or verteporfin (YAP inhibitor, 5 μM) combined with ICG-001 (antagonist of β-catenin/TCF4 binding, 5 μM) or MK-2206 (AKT inhibitor, 2 μM) for 48 h. Data are mean ± S.E.M. *P<0.05, ***P<0.001, unpaired two-tailed Student's *t*-test. **F,** Representative phase contrast images of *Cdh1*$^{-/-}$*RHOA*$^{Y42C/+}$ or *Trp53*$^{-/-}$*Kras*$^{G12D/+}$ organoids treated for 48 h with DMSO or verteporfin (5 μM), combined with ICG-001 (5 μM) or MK-2206 (2 μM). Scale bar = 100 μm. **G,** Tumor volume of *Cdh1*$^{-/-}$*RHOA*$^{Y42C/+}$ organoids injected into flanks of NSG mice and treated with DMSO, pictilisib (PI3K inhibitor, 75 mg/kg), verteporfin (100 mg/kg) or the combination (n = 8 tumors for each). Data are mean ± S.E.M. **P<0.01, ****P<0.0001, two-way ANOVA (treatment versus DMSO).

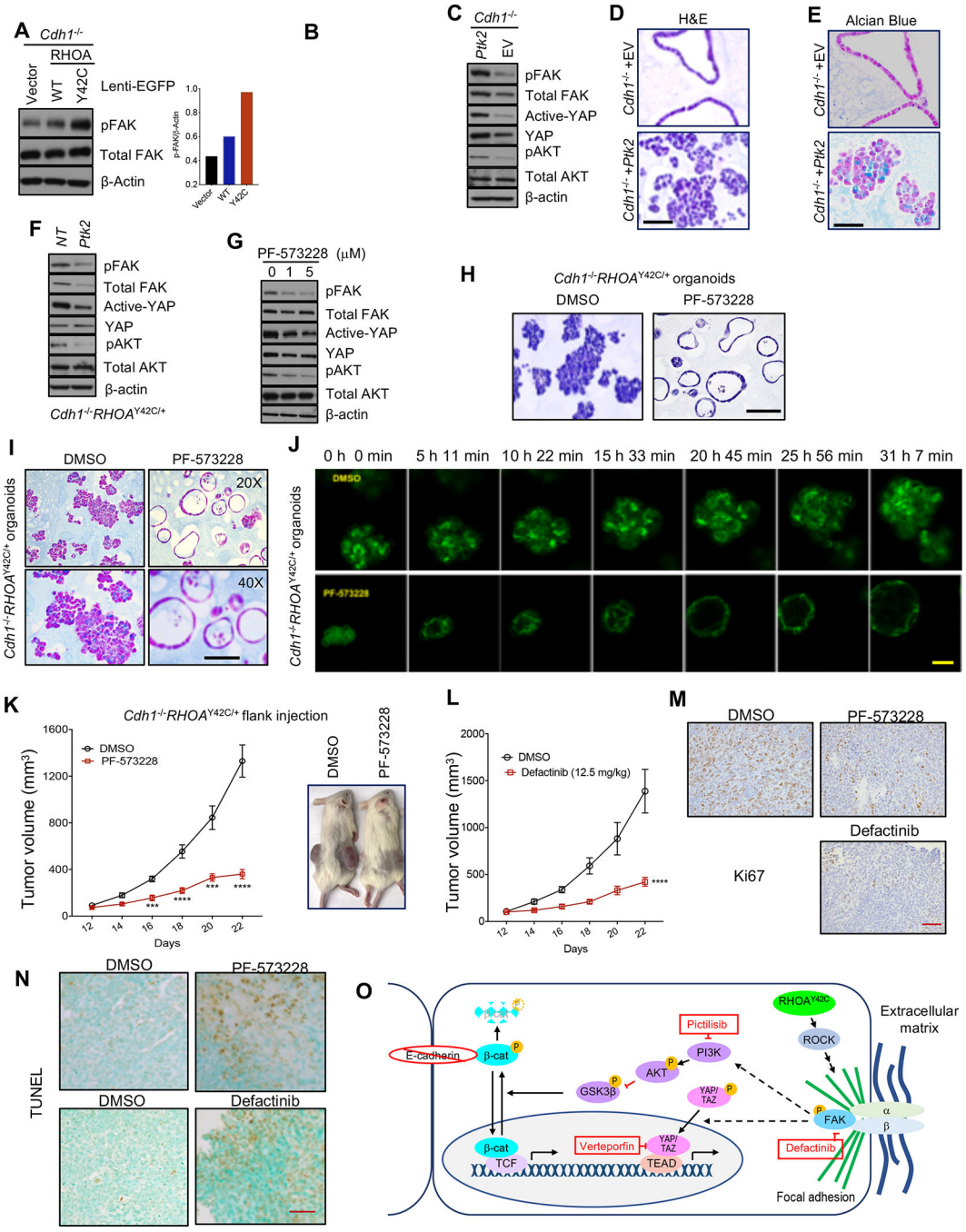

Figure 6. RHOA^{Y42C}-mediated FAK Activation Induces PI3K/AKT and YAP/TAZ.

A, Representative immunoblotting and quantitation of *Cdh1*$^{-/-}$ organoids with ectopic expression of RHOA^{Y42C}, RHOA^{WT} or EGFP control (n = 3 independent experiments). **B,** Representative immunoblotting of gastric organoids with noted genotypes (n = 3 independent experiments). **C,** Immunoblotting of *Cdh1*$^{-/-}$ organoids with ectopic expression of *Ptk2* (FAK) or vector control (n = 3 independent experiments). Representative images of H&E (**D**) and Alcian Blue (**E**) for *Cdh1*$^{-/-}$ organoids with ectopic expression of *Ptk2* or vector control. Scale bar = 100 μm. **F,** Immunoblotting of *Cdh1*$^{-/-}$*RHOA*$^{Y42C/+}$ organoids

with silencing of *Ptk2* or control (n= 3 independent experiments). **G,** Immunoblotting of *Cdh1*$^{-/-}$*RHOA*$^{Y42C/+}$ organoids treated with DMSO or PF-573228 (1 μM and 5 μM) for 48 h (n= 3 independent experiments). Representative images of (**H**) H&E and (**I**) Alcian Blue staining of *Cdh1*$^{-/-}$*RHOA*$^{Y42C/+}$ organoids treated with DMSO or PF-573228 (5 μM) for 48 h. Scale bar = 100 μm. **J,** Images from live-cell confocal microscopy of *Cdh1*$^{-/-}$*RHOA*$^{Y42C/+}$ organoids treated with DMSO or PF-573228 (5 μM), with time from drug administration marked for each image. Scale bar = 20 μm. **K,** Tumor volume of *Cdh1*$^{-/-}$*RHOA*$^{Y42C/+}$ organoids injected into flanks of NSG mice (n = 10 tumors per arm) treated with DMSO or PF-573228 (12.5 mg/kg), with representative images (right) of tumors. ***P<0.001, ****P<0.0001, unpaired two-tailed Student's t-test. Data are mean ± S.E.M. **L,** Tumor volume of *Cdh1*$^{-/-}$*RHOA*$^{Y42C/+}$ organoids injected into flanks of NSG mice (n = 10), randomly separated into 2 groups and treated with DMSO or defactinib (12.5 mg/kg) every other day. ****P<0.0001, two-way ANOVA (defactinib versus DMSO). Data are mean ± S.E.M. **M,** Representative images of Ki67 staining of tumors from (K) and (L). Scale bar = 100 μm. **N,** Representative images of TUNEL staining of tumors from (K) and (L). Scale bar = 100 μm. **O,** Model of the signaling network induced by the gain-of-function mutation RHOA^{Y42C} and loss of *Cdh1* (E-cadherin) in DGC. Targeted inhibitors are depicted in red boxes.

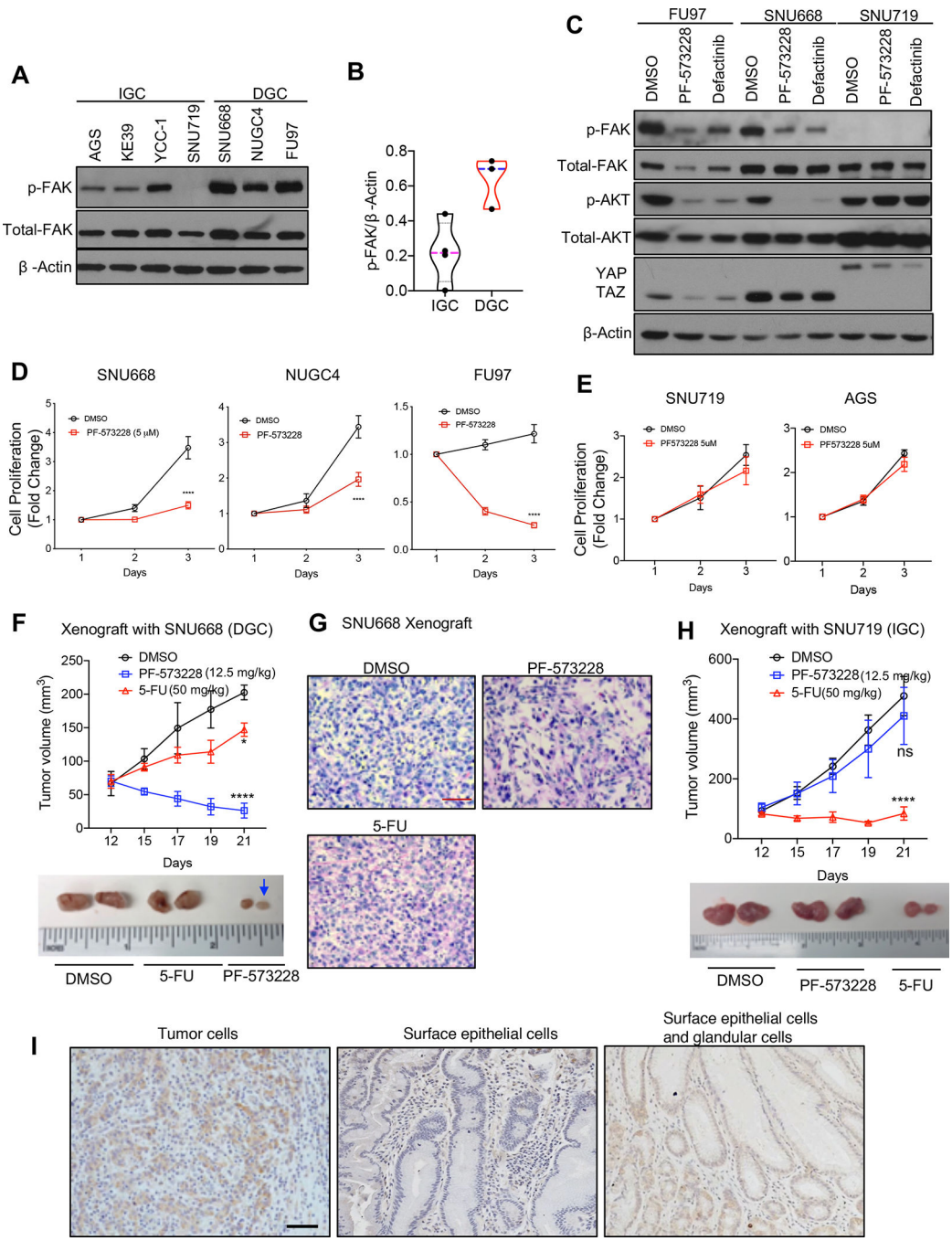

Figure 7. FAK is a potent therapeutic target in human DGC cell lines and patients.

A, Immunoblots from IGC cell lines: AGS, KE39,YCC-1 and SNU719, and DGC lines SNU668, NUGC4 and FU97 (n = 3 independent experiments). **B,** Quantification of pFAK levels from (**A**). **C,** Representative immunoblots of FU97,SNU668 and SNU719 cells treated for 24 h with DMSO or FAK inhibitor PF-573228 (5 μM) or defactinib (2.5 μM) (n = 3 independent experiments). **D,** *In vitro* proliferation of SNU668, NUGC4 and FU97 cells treated for indicated days with DMSO or PF-573228 (5 μM). Data are mean ± S.E.M. **** P<0.0001, two-way ANOVA. **E,** *In vitro* proliferation of SNU719 and AGS cells

treated for the indicated days with DMSO or PF-573228 (5 μM). Data are mean ± S.E.M. ****P<0.0001, two-way ANOVA. **F,** Tumor volume of 1×10^6 SNU668 cells injected into flanks of NSG mice and treated with DMSO (n=4) or 5-FU (n=4, 50 mg/kg) or PF-573228 (n=6, 12.5 mg/kg) every other day, with representative images (bottom) of tumors from each group. *P<0.05, ****P<0.0001, two-way ANOVA (Treatments versus DMSO). Data are mean ± S.E.M. **G,** Representative images of H&E of tumors from panel (F). Scale bar = 100 μm. **H,** Tumor volume of 1×10^6 SNU719 cells injected into flanks of NSG mice and treated with DMSO (n=4) or 5-FU (n=5, 50 mg/kg) or PF-573228 (n=4, 12.5 mg/kg) every other day. ns, not significant, ****P<0.0001, two-way ANOVA (Treatment versus DMSO). Data are mean ± S.E.M. **I,** Representative images of pFAK staining for human diffuse gastric patients with tumor area (left), adjacent normal surface epithelial area (middle) and gland epithelial cells (right). Scale bar = 100 μm.